POLITECNICO DI MILANO

Scuola di Ingegneria Industriale e dell'Informazione

Corso di Laurea Magistrale in Ingegneria Biomedica

BIOMECHANICAL CHARACTERIZATION OF PORCINE RETINA

Relatore: Prof.ssa Federica Boschetti

Correlatore: Dott.ssa Beatrice Belgio

Tesi di Laurea Magistrale di:

Sara Ragazzini

Matricola: 905502

Anno Accademico 2019/2020

Ai miei capisaldi
Mamma, Papà e Alessia
Emilia, Pietro e Nicola

Ringraziamenti

Vorrei ringraziare innanzitutto la Professoressa Boschetti e la mia tutor Beatrice. Sento di aver imparato più in questi mesi passati al Labs che in tutti gli anni al Politecnico. Vi ringrazio per la disponibilità, il supporto e soprattutto la fiducia che avete sempre mostrato nei miei confronti. È stata un'esperienza gratificante e che non dimenticherò mai.

Ringrazio inoltre il Prof. Rodriguez e il Dott. Arpa per la disponibilità mostrata nei miei confronti e in quelli di questo progetto. Grazie al Sig. Fumagalli per la sua disponibilità e gentilezza.

Un doveroso e sentito ringraziamento va alla mia famiglia. Grazie mamma e papà perché anche nei momenti in cui sbagliavo, consapevolmente e non, mi avete spronata a non mollare e mi avete ricordato quanto valessi. Grazie a mia sorella Alessia perché in quei momenti in cui sento di essere completamente inadatta mi fa sentire la persona più forte del mondo.

Ringrazio poi la mia famiglia di Milano, da Corsico 1 a Ripa 13. Forse non ci siamo scelti, ma insieme abbiamo deciso di rimanere l'uno nelle vite dell'altro. Sento che è una cosa che non cambierà mai. Colgo l'occasione per scusarmi per tutte quelle sveglie rimandate ogni mattina. Un ringraziamento speciale lo devo a Mimmi, che cinque anni fa mi ha preso la mano e da allora, con il sorriso, le lacrime o il fumo che esce dalle orecchie, non me l'ha mai lasciata.

Ringrazio Pietro e Nicola che ormai da 11 anni a questa parte non mi hanno mai abbandonata. Siamo la perfetta dimostrazione che quando i rapporti sono veri non c'è distanza, punto di vista o differenza caratteriale che possa nuocere. Che poi io in realtà penso che le nostre differenze siano proprio il nostro punto di forza.

Ringrazio i Ribelli, le persone migliori che il Politecnico potesse regalarmi. Grazie a Federica che ovunque si trovi non mi fa mai dimenticare quanto sia importante per lei. Grazie Francesca per le lacrime e le gioie condivise, grazie perché metti un impegno enorme a tenerci tutti uniti ovunque ci troviamo. Grazie Lollo per la tua razionalità, per le notti passate in patio e per quelle evasioni in certi momenti necessarie. Grazie ad Alessandro per non avermi mai fatta sentire l'unica "bullizzata". Grazie Marco perché non perdi mai occasione per ricordarci quanto OC sia fondamentale nelle nostre vite. Grazie Leonardo perché quando prendi in mano la chitarra rendi noi, tanto diversi, così simili.

Ringrazio infine me stessa, che nonostante spesso la voglia, l'intuito e la predisposizione per affrontare certi ostacoli siano mancati, oggi sono qui con voi a festeggiare questo traguardo incredibile.

Table of Contents

Table of Figures

List of Tables

Sommario

Introduzione

Questo progetto di tesi vuole concentrarsi sulle proprietà meccaniche della retina in quanto, a differenza di altre strutture appartenenti al sistema visivo come la sclera o la coroide, il suo comportamento biomeccanico non è stato esaustivamente studiato, presumibilmente a causa della fragilità del tessuto. Questa volontà nasce da considerazioni riguardanti uno stato patologico ben preciso che può interessare questa membrana: il distacco di retina. Infatti, questa malattia, rispetto ad altre, è caratterizzata da un coinvolgimento diretto della meccanica del tessuto e, nonostante possa essere trattata con varie tecniche chirurgiche, sembra che nessuna di esse possa assicurare che non si debba intervenire nuovamente. Da qui nasce l'importanza dello studio della biomeccanica della retina: conoscere le sue proprietà meccaniche significherebbe avere l'opportunità di migliorare le tecniche preesistenti, crearne di nuove o diversamente generare dei modelli computazionali che possano simulare il tessuto, la sua patologia ed il suo trattamento.

Per raggiungere l'obiettivo, è stato deciso di svolgere prove a trazione uniassiale su campioni di retina in diverse condizioni. Il processo di prova, in generale, consiste nel porre il campione tra due afferraggi e lentamente metterlo in tensione fino a raggiungerne la rottura. Successivamente, vengono calcolati i parametri biomeccanici. È di fondamentale importanza, quando si ha a che fare con i tessuti biologici, tenere in considerazione alcune problematiche come la non omogeneità del tessuto e la variabilità interindividuale, la possibilità che il tessuto possa essere danneggiato durante il suo reperimento, la sua preparazione e conservazione. Altri problemi possono essere legati all'imprecisione nel rilievo delle dimensioni del campione, fondamentali per il calcolo dei parametri meccanici e, infine al trasferimento del campione tra le due morse. Nel corso della trattazione sarà possibile vedere come si sia cercato di trovare una soluzione alla maggior parte di questi problemi, consistenti quando si parla di un campione così delicato come quello retinico.

Materiali e metodi

Con il fine di determinare le caratteristiche biomeccaniche della retina sono stati effettuati test a trazione in diverse condizioni. Le prove sperimentali sono state eseguite su campioni estratti da occhi di suino forniti dalla *Fumagalli Industria Alimentare Spa (Tavernerio, Como),* e analizzati entro circa 10 ore dalla morte dell'animale al *LaBS, Dipartimento di Chimica, Materiali e Ingegneria Chimica, Politecnico di Milano*.

In un primo momento le prove sono state effettuate tramite una prima macchina da test (TC3F, EBERS), costituita da una camera di prova smontabile con al suo interno due afferraggi: il superiore mobile e l'inferiore fisso. In questo caso, i test sono stati eseguiti su due diversi tipi di campione: retina attaccata al nervo ottico (Figura A-A), usato come afferraggio, e retina senza nervo ottico, ovvero un singolo "foglio" di retina ripiegato in 2 o 4 strati a seconda della dimensione iniziale del provino (Figura A-B). Nel secondo caso le prove sono state inoltre effettuate in presenza di tampone fosfato-salino (PBS).

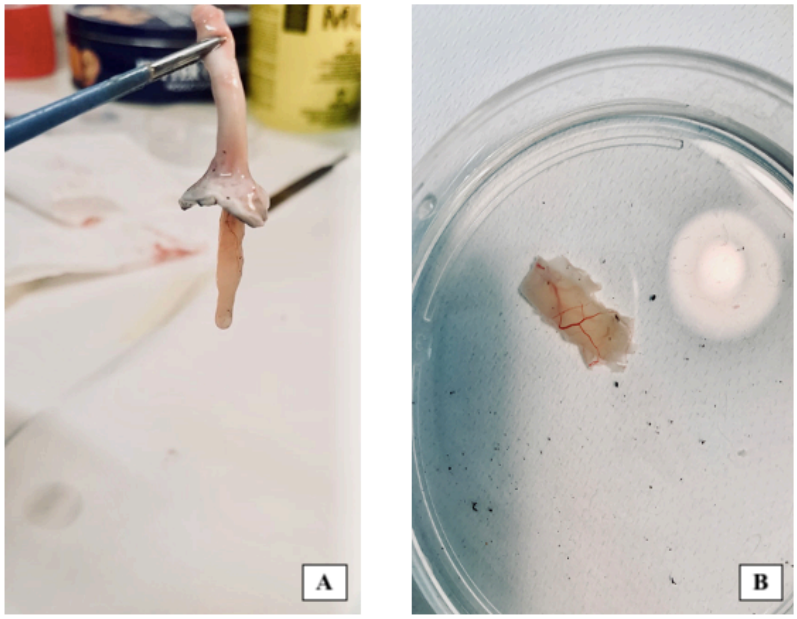

Figura A Campione di retina con nervo ottico (A) e senza nervo ottico (B)

Per quanto riguarda le dimensioni dei provini ne sono state considerate tre, essenziali per il calcolo dei parametri biomeccanici: L_0, definita come la distanza iniziale tra i due morsetti prima della partenza della prova; la larghezza, misurata tramite un calibro digitale dopo il trasferimento del campione tra gli afferraggi, e lo spessore. In questo ultimo caso l'approccio è stato diverso per i due campioni: nel caso dei provini attaccati al nervo ottico la misura è stata meno precisa con il vantaggio però di una minor difficoltà di trasferimento del campione nella camera di prova. Infatti, ciò che si ottiene a seguito del protocollo di estrazione è un agglomerato di tessuto in cui è impossibile determinare in quanti strati la retina si sia ripiegata su sé stessa. Per questo motivo la misura dello spessore è stata effettuata in maniera approssimativa con un calibro digitale come mostrato in Figura B.

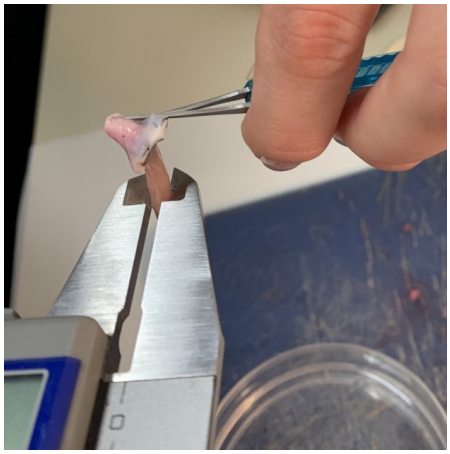

Figura B Misura dello spessore di un campione con nervo ottico tramite calibro digitale

Nel caso invece di campioni senza nervo ottico, è stato possibile stimare lo spessore con una maggior precisione. Infatti, ripiegando il campione di retina un numero noto di volte e, conoscendo lo spessore iniziale di un singolo strato, è stato possibile ottenere una misura più veritiera. Per quanto riguarda lo spessore di un singolo strato di retina il valore è stato stimato tramite Tomografia a Coerenza Ottica (OCT), una tecnica particolarmente importante in oftalmologia che permette di ottenere immagini in tempo reale delle sezioni trasversali della retina. Questo non solo permette di valutare eventuali stati patologici ma anche di ottenere misure quantitative, come mostrato in Figura C. L'analisi è stata effettuata su tre occhi di suino. Successivamente, tramite un'analisi di immagine effettuata con ImageJ sulle tre immagini tomografiche, è stato possibile ottenere un valore medio di spessore che potesse essere usato per tutti i campioni senza nervo ottico.

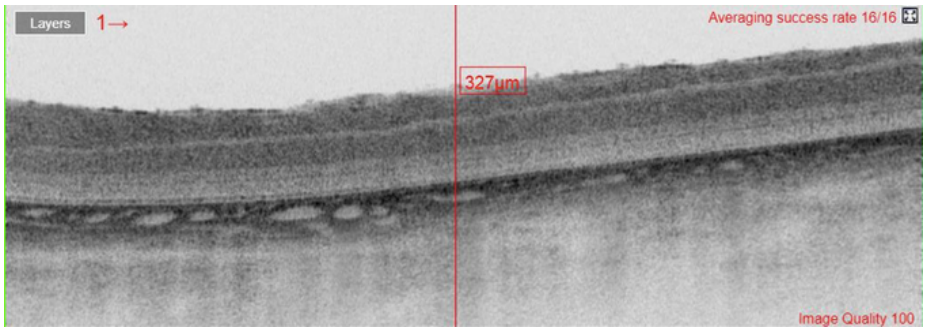

Figura C Immagine tomografica ottenuta da analisi OCT. Il numero in corrispondenza della linea rossa rappresenta lo spessore della retina in quel punto [µm]

Sono stati eseguiti 9 test per entrambi i tipi di campione, applicando una velocità di 0.1 mm/s all'afferraggio superiore della macchina da test.
Una volta effettuate le prove, il software restituisce dei parametri tra cui, in particolare, lo spostamento [mm] e la forza [N] applicati al campione. Partendo da questi vengono calcolati sforzi [kPa] e deformazioni [mm/mm] e quindi plottata la curva sforzo-deformazione dalla quale sono poi estratti il modulo di Young (E), definito come coefficiente angolare della parte lineare della curva prima del cambio di pendenza, lo sforzo di snervamento, punto in corrispondenza del quale si ha un cambiamento nell'andamento della curva, lo stress a rottura, definito come il primo valore di sforzo in cui la curva decresce in maniera evidente e, infine, la deformazione a rottura, ovvero il valore di deformazione in corrispondenza dello stress a rottura.

Per quanto riguarda i campioni senza nervo ottico, in un secondo momento, le prove sono state svolte anche con un secondo macchinario (EnduraTEC, BOSE) (Figura D), con lo scopo di mettere a confronto dati risultanti da due protocolli diversi, sebbene le modalità di estrazione dei campioni, i parametri di input e quelli di output rimanessero gli stessi. Tuttavia, in questo caso, non è stato possibile eseguire prove in presenza di PBS in quanto la camera da test preesistente si è rivelata essere inadatta al trasferimento del campione di retina tra gli afferraggi. Per questa ragione, uno degli step finali di questo progetto di tesi ha previsto la progettazione di una nuova camera che superasse i limiti della prima e, in particolare, che permettesse di montare il campione senza danneggiarlo. Le prove sono state effettuate su un numero totale di 16 provini di retina e i parametri calcolati sono stati gli stessi delle prove precedentemente descritte.

Figura D Macchina da test EnduraTEC, BOSE

Alla fine delle prove è stata effettuata un'analisi statistica sui parametri biomeccanici calcolati. In particolare, per ogni parametro preso in considerazione sono state calcolate tramite Excel media e deviazione standard. I valori sono stati poi confrontati con quelli presenti in letteratura. Inoltre, tra le due famiglie di campioni analizzati con la macchina TC3F, è stato effettuato un t-student test tra i valori del modulo di Young con il fine di determinare se l'uso del nervo ottico come afferraggio potesse influenzare le proprietà meccaniche della retina.

A seguito di alcune differenze evidenziate tra i valori di deformazione calcolate al termine delle prove di trazione eseguite con le macchine TC3F ed EnduraTEC, è stato ritenuto opportuno effettuare un'ulteriore analisi. La Digital Image Correlation (DIC), è un'analisi ottica non invasiva che permette di misurare gli spostamenti e le deformazioni sulla superfice di oggetti soggetti a sollecitazione. Essa si basa sul monitoraggio di dettagli unici presenti sulla superfice del campione tramite elaborazione numerica di immagini digitali: analizzando i valori di grigio di diversi frame, le deformazioni e gli spostamenti possono essere quantificati tramite un algoritmo di correlazione. Per applicare l'analisi ai nostri campioni è stato necessario creare sulla loro superficie un pattern il più uniforme possibile e questo è stato possibile grazie all'uso di toner in polvere su di uno spazzolino da denti.

Risultati

Di seguito vengono riportati i risultati derivanti da ciascuna analisi effettuata nel corso di questo progetto di tesi. Per le prove meccaniche si riportano esclusivamente i valori medi dei parametri biomeccanici calcolati a seguito dei diversi test eseguiti.

La tabella A riporta il valore medio dello spessore stimato a seguito dell'analisi di immagine sulle immagini derivanti dall'OCT e la sua deviazione standard. Il valore ottenuto si inserisce perfettamente nel range di valori presenti in letteratura (300-400 μm) [19] e questo rende l'OCT una tecnica di misurazione alternativa a quelle presenti in altri lavori valida ed efficace.

Valore Finale Spessore Medio [μm]	Deviazione Standard
351.75	38.45

Tabella A Valore finale di spessore medio e deviazione standard

Per quanto riguarda le prove sperimentali, la Figura E mostra una delle curve sforzo deformazione ottenute a seguito di test eseguiti con la macchina da test TC3F. L'andamento è caratterizzato da una breve fase iniziale lineare seguita da una plastica più ampia. La linea arancione rappresenta il tratto considerato per il calcolo del modulo di Young.

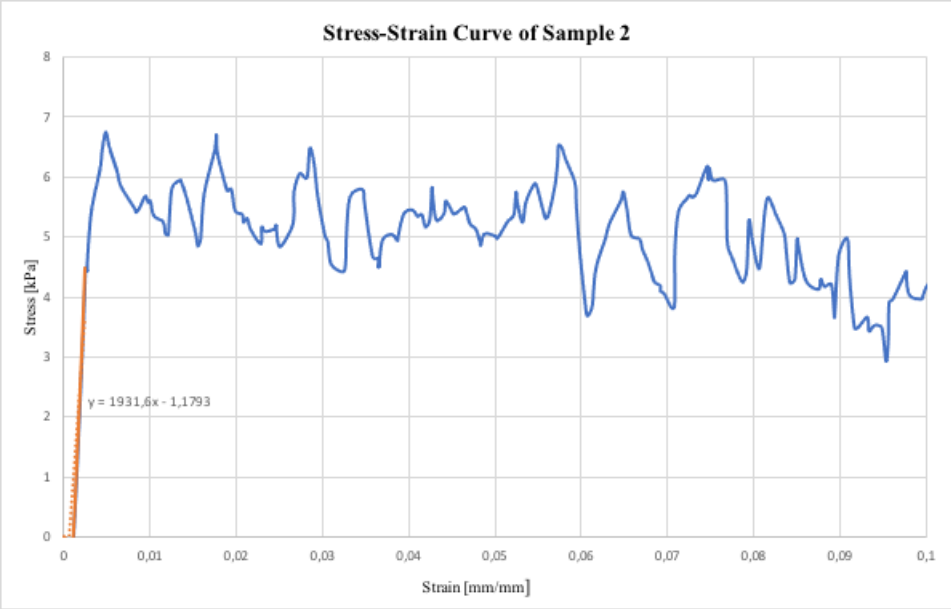

Figura E Curva sforzo-deformazione di una campione con nervo ottico analizzato con la macchina TC3F. Sull'asse x le deformazioni sono espresse in [mm/mm] mentre sull'asse y gli sforzi sono espressi in [kPa].

Le Tabelle B e C riportano i valori medi dei parametri biomeccanici calcolati a seguito delle prove a trazione eseguite con la macchina da test TC3F rispettivamente su campioni con nervo ottico e senza.

Modulo di Young Medio [kPa] ± SD	1835 ± 1.35
Sforzo di Snervamento Medio [kPa] ± SD	3.03 ± 2.23
Sforzo a Rottura Medio [kPa] ± SD	7.46 ± 5.8
Deformazione a Rottura Media [mm/mm] ± SD	0.089 ± 0.1

Tabella B Valori medi dei parametri biomeccanici calcolati per campioni con nervo ottico e deviazione standard

Modulo di Young Medio [kPa] ± SD	3470 ± 3.09
Sforzo di snervamento medio [kPa] ± SD	9.15 ± 6.09
Sforzo a Rottura Medio [kPa] ± SD	9.76 ± 6.1
Deformazione a Rottura Media ± SD	0.113 ± 0.2

Tabella C Valori medi dei parametri biomeccanici calcolati per campioni senza nervo ottico e deviazione standard

Per entrambe le tipologie di prova, gli andamenti delle curve ottenute sono coerenti con quelli presenti in letteratura. Tuttavia, per entrambi i campioni, i valori di deformazione risultano essere molto bassi e questo influenza chiaramente i valori dei parametri biomeccanici: in particolare il modulo di Young risulta essere 1-2 ordini di grandezza maggiore rispetto allo stato dell'arte. Questo potrebbe essere dovuto al fatto che il software non acquisisce un numero di punti sufficiente a caratterizzare il tessuto in maniera soddisfacente.

È stato inoltre svolto un t-test con il fine di determinare se l'uso del nervo ottico come afferraggio potesse influenzare le proprietà meccaniche della retina e, in particolare, il valore del modulo di Young. I risultati dimostrano che i due protocolli portano a risultati privi di differenza significativa ($P>0.05$)

Infine, per quanto riguarda i test a trazione, la Figura F mostra una delle curve ottenute a seguito dei test effettuati sui campioni senza nervo ottico con la macchina EnduraTEC. Anche in questo caso la curva è caratterizzata da una breve fase elastica lineare seguita da una regione plastica più ampia.

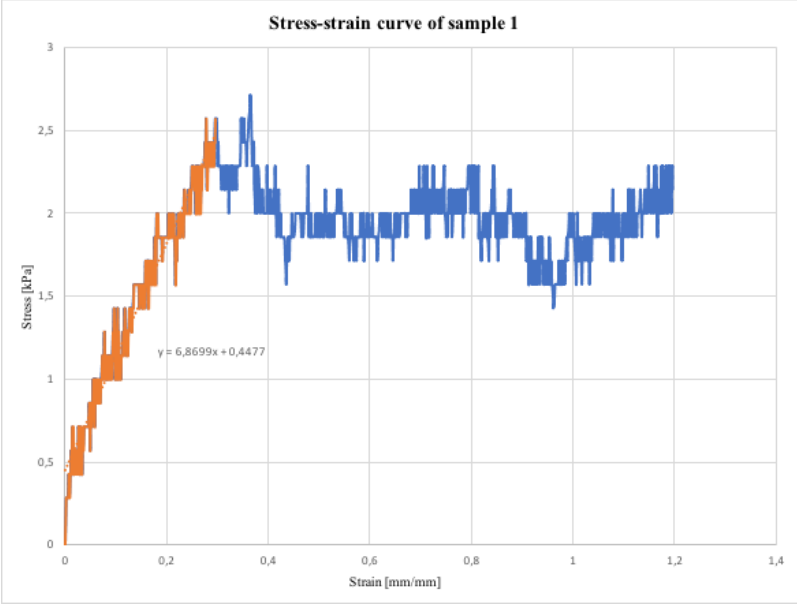

Figura F Curva sforzo-deformazione di una campione senza nervo ottico analizzato con la macchina EnduraTEC. Sull'asse x le deformazioni sono espresse in [mm/mm] mentre sull'asse y gli sforzi sono espressi in [kPa]

La Tabella D riporta i parametri biomeccanici medi calcolati per questo tipo di prova.

Modulo di Young Medio [kPa] ± SD	13.4 ± 0.0067
Sforzo di Snervamento Medio [kPa] ± SD	1.33 ± 0.75
Sforzo a Rottura Medio [kPa] ± SD	2.21 ± 0.8
Deformazione a Rottura Media [mm/mm] ± SD	0.66 ± 0.3

Tabella D Valori medi dei parametri biomeccanici calcolati per campioni senza nervo ottico e deviazione standard

Le prove effettuate con la EnduraTEC non solo hanno restituito andamenti delle curve coerenti con quelli in letteratura, ma anche i valori dei parametri biomeccanici si sono rivelati essere in linea con quelli dei precedenti lavori.

Per quanto riguarda infine l'analisi DIC siamo in possesso di soli risultati preliminari e in particolare, si riporta di seguito la mappa colorimetrica delle deformazioni, in configurazione Euleriana, considerate nella direzione della forza applicata (Figura G). I valori di deformazione sono in linea con quelli derivanti dalle prove sperimentali svolte con l'EnduraTEC.

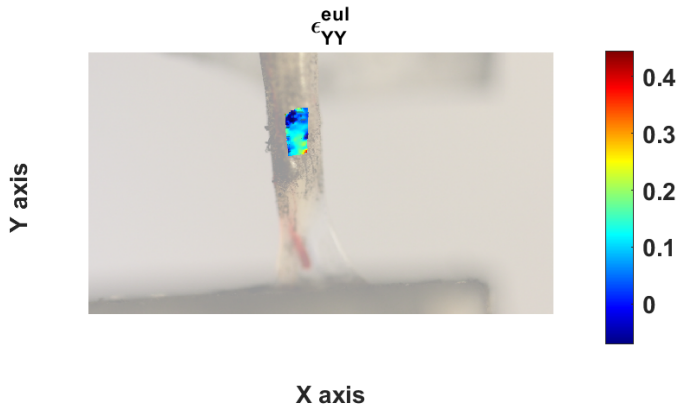

Figura G Mappa colorimetrica rispetto alla componente Euleriana ε_{yy}

Conclusioni

Lo scopo principale di questo progetto di tesi è stato quello di eseguire una caratterizzazione biomeccanica della retina suina partendo da considerazioni fatte sul distacco di retina, una condizione patologica in cui la meccanica del tessuto è direttamente coinvolta. Conoscere le proprietà biomeccaniche di questo tessuto vorrebbe quindi dire avere la possibilità di migliorare le tecniche chirurgiche preesistenti o crearne di nuove.

In conclusione, possiamo dire che i parametri biomeccanici ottenuti a seguito delle analisi svolte sono coerenti con quelli presenti in letteratura che definiscono la retina un tessuto fragile con un comportamento biomeccanico caratterizzato da una breve fase elastica seguita da una fase plastica più ampia.

Abstract

Introduction

This thesis project aims to focus on the mechanical properties of the retina since, differently from other structures belonging to the visual system such as the sclera or the choroid, its biomechanical behavior has not been exhaustively studied, presumably due to the fragility of the tissue. This will was born from considerations regarding a very specific pathological state that can affect this membrane: the retinal detachment. In fact, this disease, compared to others, is characterized by a direct involvement of the mechanics of the tissue and, although it can be treated with various surgical techniques, it seems that none of them can ensure that no further intervention is required. Hence the importance of the study of the biomechanics of the retina: knowing its mechanical properties would mean having the opportunity to improve existing techniques, create new ones or otherwise generate computational models that can simulate the tissue, its pathology and its treatment.

To achieve this goal, it was decided to perform uniaxial tensile tests on retinal samples under different conditions. The testing process, in general, consists of placing the sample between two grips and slowly tensioning it until it breaks. Then, biomechanical parameters are calculated.

It is of fundamental importance, when dealing with biological tissues, to take into consideration some problems such as the non-homogeneity of the tissue and the inter-individual variability, the possibility that the tissue can be damaged during its retrieval, preparation and conservation. Other problems may be related to the imprecision in the measurement of the sample dimensions, fundamental for the calculation of the mechanical parameters and, finally, to the transfer of the sample between the two clamps. In the course of the discussion it will be possible to see how we tried to find a solution to most of these problems, which are consistent when we are talking about such a delicate sample as the retinal one.

Materials and methods

In order to determine the biomechanical characteristics of the retina, tensile tests were carried out in different conditions. The experimental tests were performed on samples extracted from pig eyes supplied by *Fumagalli Industria Alimentare Spa* (Tavernerio, Como), and analyzed within about 10 hours of the animal's death at *LaBS, Department of Chemistry, Materials and Chemical Engineering*, Politecnico di Milan.

At first the tests were performed using a first test machine (TC3F, EBERS), consisting of a demountable test chamber with two grips inside: the upper mobile and the lower fixed. In this case, the tests were performed on two different types of sample: retina attached to the optic nerve (Fig.A-A), used as a grasp, and retina without an optic nerve, i.e. a single "sheet" of retina folded into 2 or 4 layers depending on the size initial of the specimen (Fig.A-B). In the second case, the tests were also carried out in the presence of phosphate-buffer-saline solution (PBS).

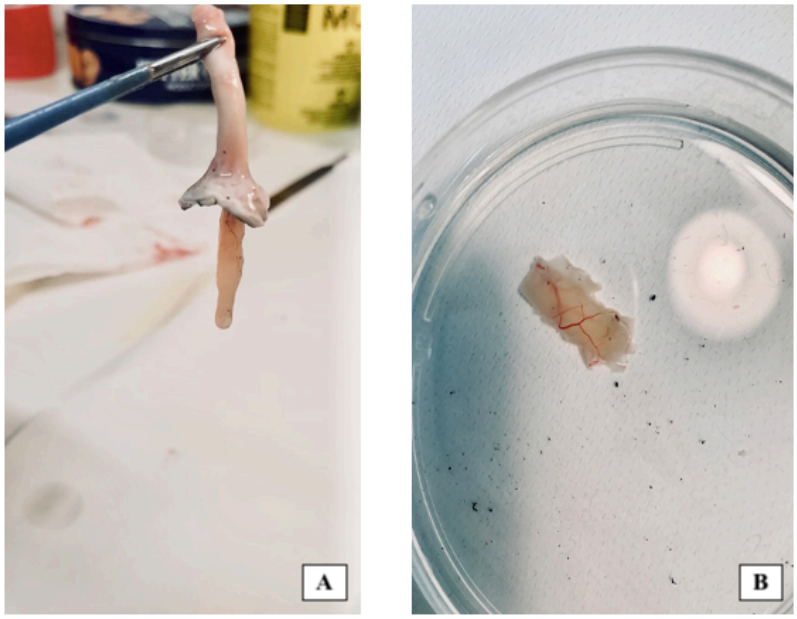

Fig. A Sample of retina with optic nerve (A) and without optic nerve (B)

As regards the dimensions of the specimens, three were considered, essential for the calculation of the biomechanical parameters: L0, defined as the initial distance between the two clamps before the start of the test; the width, measured by a digital caliper after the sample is transferred between the grips, and the thickness. In this last case, the measurement was different for the two types of sample: in the case of the specimens attached to the optic nerve, the measurement was less precise with the advantage, however, of less difficulty in transferring the sample to the test chamber. In fact, what is obtained following the extraction protocol is an agglomeration of tissue in which it is impossible to determine in how many layers the retina has folded back on itself. For this reason, the thickness measurement was carried out roughly with a digital caliper as shown in Fig. B.

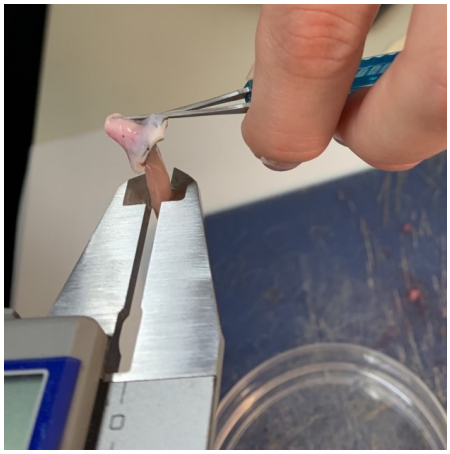

Fig. B Measurement of the thickness of a sample with optic nerve through a digital

In the case of samples without optic nerve, it was possible to estimate the thickness with greater precision. In fact, by folding the retina sample a known number of times and, knowing the initial thickness of a single layer, it was possible to obtain a more truthful measurement. As for the thickness of a single retinal layer, the value was estimated by Optical Coherence Tomography (OCT), a particularly important technique in ophthalmology that allows to obtain real-time images of the cross sections of the retina. This not only allows to evaluate any pathological states but also to obtain quantitative measures, as shown in Fig. C. The analysis was carried out on three pig eyes. Subsequently, through an image analysis carried out with ImageJ on the three tomographic images, it was possible to obtain an average thickness value that could be used for all samples without optic nerve

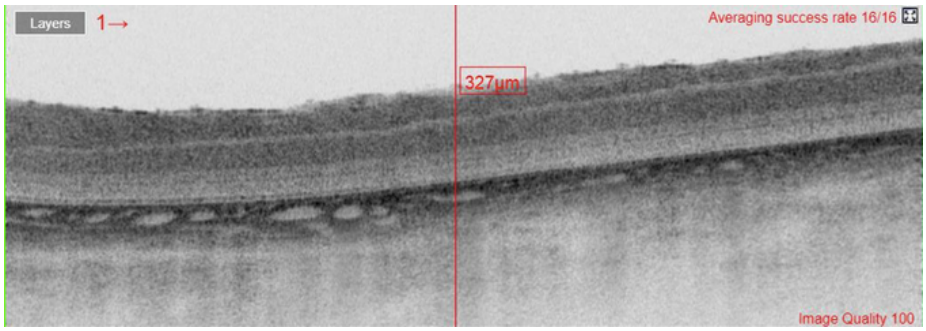

Fig. C Tomographic image obtained from OCT analysis. The number in correspondence of the red line represents the retinal thickness in that point [µm]

9 tests were performed for both types of samples, applying a speed of 0.1 mm / s to the upper grip of the test machine.

Once the tests have been carried out, the software returns parameters including, in particular, the displacement [mm] and the force [N] applied to the sample. Starting from these, stresses [kPa] and strains [mm / mm] are calculated and then the stress-strain curve is plotted. From this the Young's modulus (E), defined as the angular coefficient of the linear part of the curve before the change of slope; the yield stress, the point at which there is a change in the trend of the curve; the stress at break; defined as the first stress value in which the curve clearly decreases and, finally, the deformation at break , that is the deformation value corresponding to the stress at break, are extracted

As regards the samples without optic nerve, at a later time, the tests were also carried out with a second machine (EnduraTEC, BOSE) (Fig.D), with the aim of comparing data resulting from two different protocols, although the methods of extraction of the samples, input parameters and output parameters remained the same. However, in this case, it was not possible to perform tests in the presence of PBS as the pre-existing test chamber was found to be unsuitable for transferring the retinal specimen between the grips. For this reason, one of the final steps of this thesis project involved the design of a new chamber that exceeded the limits of the first and, in particular, that would allow the sample to be mounted without damaging it. The tests were carried out on a total number of 16 retinal specimens and the calculated parameters were the same as the previously described tests.

Fig. D Tensile test machine EnduraTEC, BOSE

At the end of the tests, a statistical analysis was carried out on the calculated biomechanical parameters. In particular, the mean and standard deviation were calculated using Excel for each parameter taken into consideration. The values were then compared with those present in the literature. Moreover, between the two families of samples analyzed with the TC3F machine, a t-student test was carried out between the values of the Young's modulus in order to determine whether the use of optic nerve such as grasping could affect the mechanical properties of the retina.

Following some differences highlighted between the deformation values calculated at the end of the tensile tests performed with the TC3F and EnduraTEC machines, it was deemed appropriate to carry out a further analysis. Digital Image Correlation (DIC) is a non-invasive optical analysis that allows you to measure displacements and deformations on the surface of objects subject to stress. It is based on the monitoring of unique details present on the sample surface through numerical processing of digital images: by analyzing the gray values of different frames, the deformations and displacements can be quantified through a correlation algorithm. To apply the analysis to our samples it was necessary to create a pattern on their surface as uniform as possible and this was possible thanks to the use of toner powder on a toothbrush.

Results

The results deriving from each analysis carried out during this thesis project are reported below. For the mechanical tests, only the average values of the biomechanical parameters calculated following the various tests performed are reported.

Tab. A reports the final average value of the retinal thickness obtained after the image analysis performed on the tomographic images resulting from OCT.
It fits perfectly into the range of values found in the literature (300-400 μm) [19] and this makes OCT a valid and effective alternative measurement technique to those present in other works.

Final Average Value of Retinal Thickness[μm]	Standard Deviation
351.75	38.45

Tab. A Final average value of retinal thickness and standard deviation

As for the experimental tests, Fig. E shows one of the stress-strain curves obtained following a tensile test performed with the TC3F test machine. The trend is characterized by a short linear initial phase followed by a larger plastic one. The orange line represents the section considered for the calculation of Young's modulus.

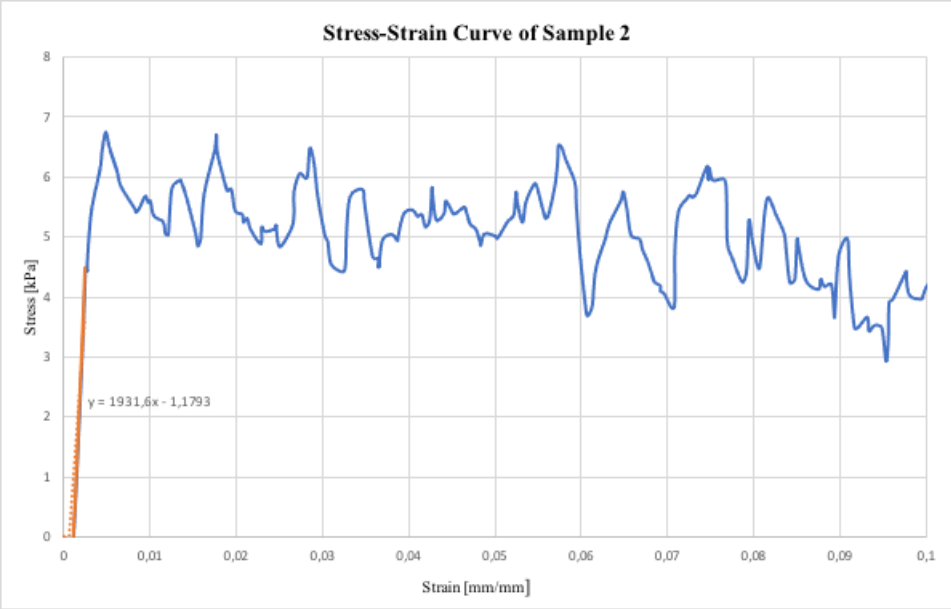

Fig. E Stress-strain curve of a sample with optic nerve. On x-axis the strains are reported in [mm/mm] while on y-axis stresses are reported in [kPa]

Tab. B and C report the average values of the biomechanical parameters calculated following the tensile tests carried out with the first machine on samples with and without optic nerve respectively.

Average Young's Modulus [kPa] ± SD	1835 ± 1.35
Average Yield Stress [kPa] ± SD	3.03 ± 2.23
Average Failure Stress [kPa] ± SD	7.46 ± 5.8
Average Failure Strain [mm/mm] ± SD	0.089 ± 0.1

Tab. B Average values of the biomechanical parameters calculated for samples with optic nerve and standard deviation

Average Young's Modulus [kPa] ± SD	3470 ± 3.09
Average Yield Stress [kPa] ± SD	9.15 ± 6.09
Average Failure Stress [kPa] ± SD	9.76 ± 6.1
Average Failure Strain [mm/mm] ± SD	0.113 ± 0.2

Tab. C Average values of the biomechanical parameters calculated for sample without optic nerve and standard deviation

For both types of tests, the trends of the curves obtained are consistent with those present in the literature. However, for both samples, the deformation values are very low, and this clearly affects the values of the others biomechanical parameters: in particular, Young's modulus is 1-2 orders of magnitude greater than the state of the art. This could be due to the fact that the software does not acquire a sufficient number of points to characterize the tissue satisfactorily.

A t-test was also carried out in order to determine if the use of the optic nerve as grasping could influence the mechanical properties of the retina and, in particular, the value of Young's modulus. The results demonstrate that the two protocols lead to results with no significant difference (P>0.05).

Finally, as regards the tensile tests, Fig. F shows one of the curves obtained following the tests carried out on samples without optic nerve with the EnduraTEC machine. Again, the curve is characterized by a short linear elastic phase followed by a wider plastic region.

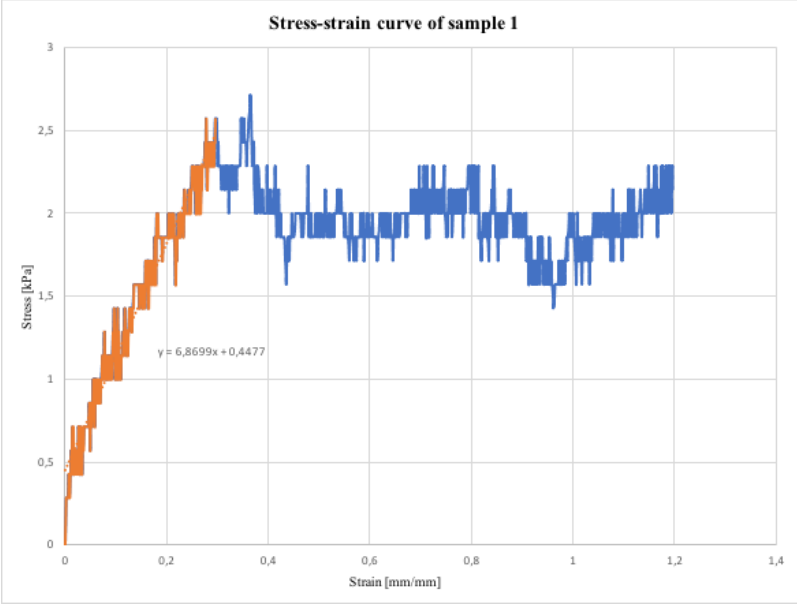

Fig. F Stress-strain curve of a sample without optic nerve. On x-axis the strains are reported in [mm/mm] while on y-axis stresses are reported in [kPa]

Finally, Tab. D reports the average biomechanical parameters calculated for this type of test.

Average Young's Modulus [kPa] ± SD	13.4 ± 0.0067
Average Yield Stress [kPa] ± SD	1.33 ± 0.75
Average Failure Stress [kPa] ± SD	2.21 ± 0.8
Average Failure Strain [mm/mm] ± SD	0.66 ± 0.3

Tab. D Average values of the biomechanical parameters calculated for sample without optic nerve and standard deviation

The tests carried out with the EnduraTEC not only returned curves consistent with those in the literature, but also the values of the biomechanical parameters proved to be in line with those of the previous works.

Finally, as regards the DIC analysis, we have only preliminary results and in particular, the following in Fig. G is the colorimetric map of the deformations, in Eulerian configuration, considered in the direction of the applied force. The deformation values are in line with those resulting from the experimental tests carried out with the EnduraTEC.

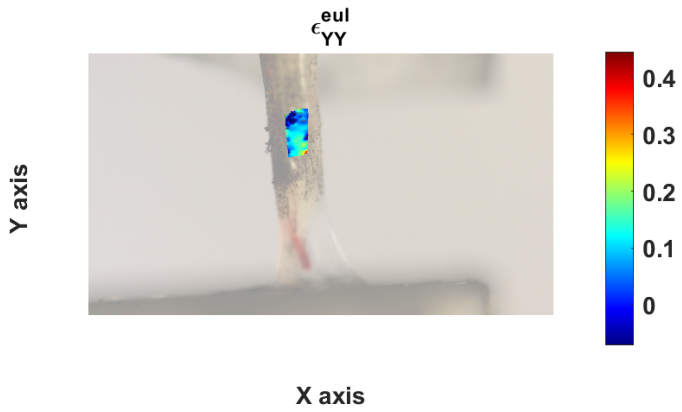

Fig. G Colorimetric map with respect to the Eulerian component εyy

Conclusions

The main purpose of this thesis project was to perform a biomechanical characterization of the porcine retina starting from considerations made on retinal detachment, a pathological condition in which the mechanics of the tissue is directly involved. Knowing the biomechanical properties of this tissue would therefore mean having the opportunity to improve pre-existing surgical techniques or create new ones.

In conclusion, we can say that the biomechanical parameters obtained following the analyzes carried out are consistent with those present in the literature which define the retina as a fragile tissue with a biomechanical behavior characterized by a short elastic phase followed by a larger plastic phase.

Chapter 1: Introduction

1.1 The Retina

The main organ of the visual system is the eye which is responsible for obtaining information from the surrounding environment through light, which is subsequently processed and sent to the brain where it is converted into an image. When the light beam reaches the eye, whose structure is schematized in Figure 1, the light intensity is regulated through a diaphragm, the iris. Then a system of lenses, the cornea and the crystalline, focuses the beam towards the retina which then converts the light information into electrical signals that will be sent to the brain through the optic nerve, processed and interpreted.

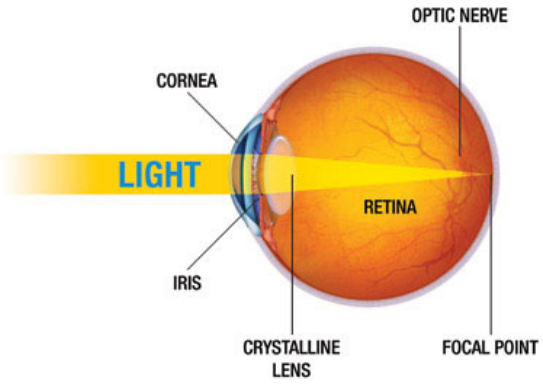

Figure 1 Eye Structure

The *retina* remains the most studied part of the human brain. It is considered embryologically as part of the central nervous system [1-3], but readily accessible to examination, it can be investigated with relative ease by both scientists and clinicians [14]. This work focuses precisely on the retina and, in particular, on its biomechanical characteristics. Infact, in contrast to other eye structures like sclera and choroid, the biomechanical behavior of the retina has not received much attention, presumably because of its structural fragility [26].

First of all, before dealing with retinal biomechanics, an overview of the retina from an anatomical, physiological and pathological point of view will be made in this paragraph.

1.1.1 Anatomy

The retina is the innermost membrane of the eyeball and represents the main component for vision thanks to the ability to convert the luminous radiation into electrical potential due to the presence of two types of photoreceptors: the cones and the rods. For this reason, it is considered the neurosensory component of the eye [14]. In particular, the retina forms the inner coating of the entire eyeball, from the starting point of the optic nerve to the pupillary margin of the iris, with a thickness varying between 0.4 and 0.1 mm respectively. Its outer part is supplied by a vascular layer, the choroid, and protect by a tough outer layer, the sclera [14].

The retina is divided into three portions: the *optical part*, applied to the choroid; the *ciliary part*, adherent to the ciliary body and the *iris part*. Among these, the only portion responsible for vision is the optical part due to the presence of the photoreceptors. The optical part can be divided into two sheets: the outer most is the layer of the pigmented cells, including photoreceptors and pigmented epithelial cells, while the inner one represents the nervous portion containing neuronal and glial cells.

In addition, within the retina it is possible to distinguish three important physical elements, shown in Figure 2.

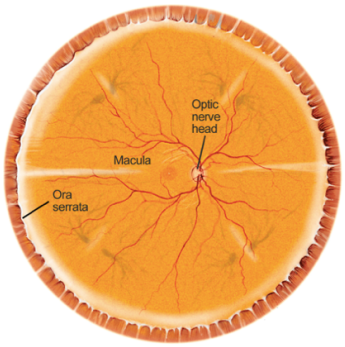

Figure 2 The three regions of the retina

The *ora serrata* is the line between the optical part and the ciliary part of the retina. It is located 6-7 mm behind the cornea and is the region in which the retina starts to change its structure thinning.

The *optic disk (papilla ottica)* is the point of convergence of the nerve fibers that will form the optic nerve and also the region from which retinal vessels emerge. It is a blind spot, being devoid of photoreceptors.

Finally, the *macula* is a region located in the posterior pole of the eye and crossed in the center by the visual axis of the eye. This central point of passage is called *fovea*, the area of best visual definition, in which the greatest number of light rays is concentrated, and which allows the most distinct and precise vision.

1.1.1.1 Retinal layers

The vertebrate retina, in the optical part, is divided into ten distinct layers in which the cellular elements are arranged and adapted to meet the functional requirements of the different regions of the retina [14].

Figure 3 shows a schematic representation of the layers of the retina and the respective cells. The different layers are described below starting from the outermost, the closest to the choroid, towards the innermost, closest to the vitreous body.

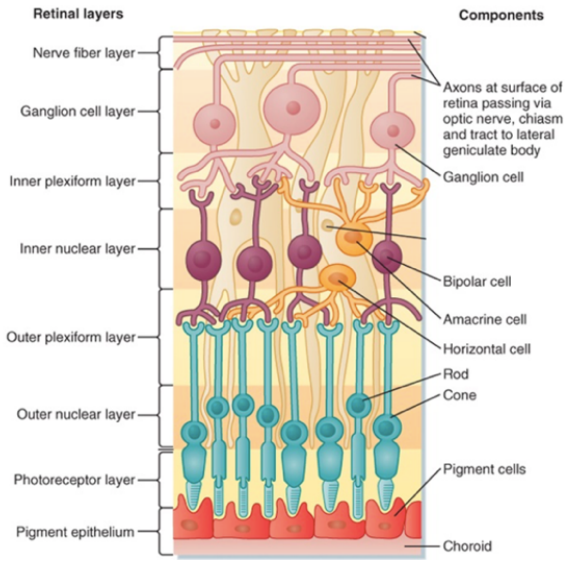

Figure 3 Schematic representation of retinal layers and retinal cell populations

The *retinal pigment epithelium (RPE)* is a single layer of cuboidal epithelial cells that adheres to the choroid and provides nourishment and supportive functions to the neurosensory retina. The pigmentation of these cells allows to absorb the light rays that are not converted by the photoreceptors to avoid the reflection of light. Moreover, it forms the blood-retina barrier which regulates the exchanges between blood and retinal tissues [6-11].

The *photoreceptors layer* is composed by the outer and inner segments of the photoreceptor cells. As mentioned before, there are two types of photoreceptors: the *cones*, responsible for color vision, and the *rods*, involved in monochromatic vision in low light conditions. In human retina we can find three different types of cones:

- *S-cones* with an absorption peak around 430 nm, sensitive to blue-violet color;
- *M-cones* with an absorption peak around 530 nm, sensitive to green color;
- *L-cones* with an absorption peak around 570 nm, sensitive to red range.

The photoreceptors are the sensors of the visual system that capture photons and convert them into a nerve signal in a process called phototransduction [16]. In particular, the human retina contains approximately 4-5 million cones and 77-107 million rods [12-14].

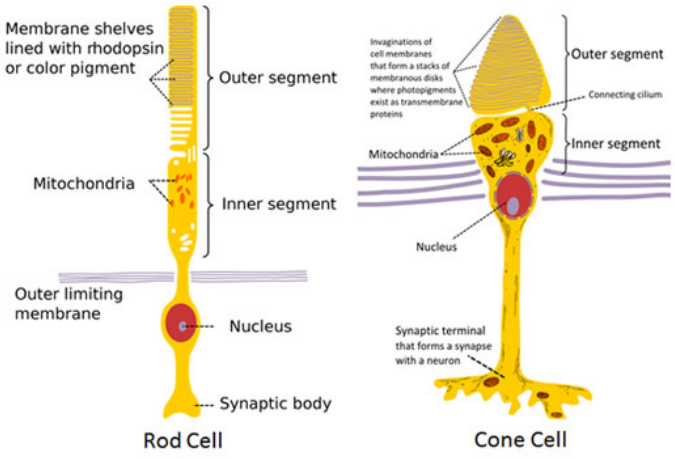

Figure 4 Rods and cones structure

Each photoreceptor (Figure 4) consists of an outer segment (photopigment), inner segment (mitochondria, endoplasmic reticulum), a nucleus, an inner fiber (analogous to an axon) and a synaptic terminal [21]. The outer segments contain the photon-capturing photopigment [14]. So, in the outer segment, the light radiation causes a reversible chemical modification of the visual pigment and the creation of an electrical potential, which is transmitted to the bipolar cells and, subsequently, to the ganglionic one.

The *external limiting membrane* is a network-like structure which separates the inner segment portions of the photoreceptors from their cell nuclei.

The *outer nuclear layer* contains the cellular bodies of cones and rods.

The *outer plexiform layer* is the first synaptic zone. This layer is formed by projections of rods and cones ending in the *rod spherule* and *cones pedicles*, respectively. These establish synapses with dendrites of bipolar and horizontal cells [21].

The *inner nuclear layer* contains the nuclei and surrounding cell bodies of neurons such as amacrine cells, bipolar cells and horizontal cells.

The *inner plexiform layer* is the second retinal processing layer with networks between bipolar or amacrine cells and ganglion cells [14].

The *ganglion cell layer* contains nuclei of the ganglion neural cells, whose axons become the optic nerve fibers, and some displaced amacrine cells [21].

The *nerve fiber layer* contains the axons of the ganglion cell bodies.

Finally, the *inner limiting membrane*, is the basement membrane produced by Müller cells. Vitreous collagen fibrils insert into this membrane of the retina, so rendering the retina vulnerable to vitreoretinal traction forces [4].

1.1.1.2 Retinal vascularization

As said, the retina is stratified into different layers, each containing specific cell types or cellular compartments with different nutritional requirements [29]. In order to satisfy these requirements, the ophthalmic artery bifurcates and supplies the retina through two distinct vascular networks: the *retinal network* and the *choroidal network* (choriocapillaris system).

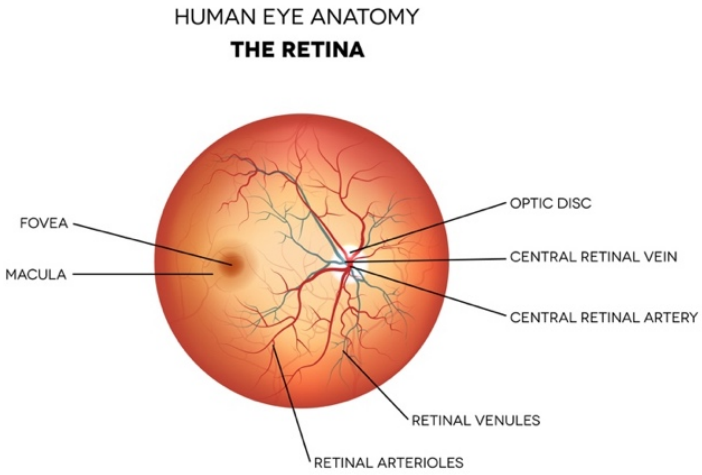

Figure 5 Retinal main vessels

In the *retinal network* the central retinal artery, the red one in Figure 5, penetrates the eye through the papilla ottica and splits into four branches that diverge towards the periphery where they further divide. The blood containing waste products goes, through four veins branches, towards the papilla and flows out of the globe through the central vein of the retina. This network supplies nourishment to ganglion and bipolar cells and the layer of nerve fibers.

On the other hand, the retinal pigment epithelium layer and, through this, the photoreceptors are supplied by the *choroidal network*, which is composed by very large lumen and loose walls capillaries. For this reason, the filtration processes are abundant and poorly selective. The oxygenated blood flows through the posterior ciliary arteries, which form a kind of arterial ring around the head of the optic nerve, whereas the deoxygenated blood flows towards four or more vascular gaps (swirling veins).

1.1.2 Function

The retina is the structure of the eyeball used to capture the light stimuli that come from the outside and convert them into nerve signals that are sent, through the optic nerve, to the brain structures responsible for visual interpretation.

From a functional point of view the retinal layers can be reduced to three:

- Pigment epithelium and photoreceptors layer;
- Bipolar, horizontal and amacrine cells layer;
- Ganglion cells layer.

The starting point of the conversion process is performed by the photoreceptors: when the light radiation reaches the retina, photochemical reactions are activated. Indeed, when cones and rods are exposed to intense or weak light respectively, they are subject to conformational changes that cause the release of neurotransmitters which will excite, or inhibit, bipolar cells which, in turn, will send potentials to ganglion cells. The axonic extensions of the ganglion cells constitute the optic nerve which will have the task of conveying the signal out of the retina to the lateral geniculate body and the cortical areas of the brain, where visual information is processed.

Amacrine and horizontal cells modulate communication in the retinal nerve tissue.

1.1.3 Retinal detachment

The retina can be affected by various pathologies characterized, for example, by morphological and structural changes due to age or trauma. Among all retinal pathologies this research project intends to focus on retinal detachment, starting point of our considerations. The reason is to be found in the fact that retinal detachment is one of those pathological conditions in which the mechanics of the biological tissue is directly involved. Knowing the mechanical properties of the retina therefore means, in this case, having the

opportunity to implement pre-existing surgical techniques, create them *ex novo* or generate computational models that can simulate the pathology and its treatment.

This disease, mainly due to a trauma, concerns limited regions of retina, but generally tends to extend progressively and affect ever larger portions of the retina, thus causing the onset of a "dark area" that extends from the periphery towards the central portion of the visual field and leading to blindness [1]. As there is no drug therapy for retinal detachment, the gold standard procedure for treating retinal detachment is represented by urgent surgery.

1.1.3.1 Types, causes and diagnosis

Retinal detachment is a really serious disorder which occurs when the neural retina separates from the layer underneath, the RPE [11]. In this condition, retinal cells remain oxygen-free which can result in cell death and consequent total loss of vision. Symptoms include an increase in the number of floaters, flashes of light and worsening of the outer part of the visual field [10].

Retinal detachment can occur for various reasons among which the most common are:

- *Posterior vitreous detachment:* it represents the most common case and it is often related to the aging. Since the vitreous body is attached to the retina, its detachment can exert traction on the retina itself, causing it to detach from the RPE layer.
- *Severe myopia:* people with sever myopia, greater than 5-6 diopters, present the greatest risk of developing retinal detachment because they often have thinner retinas [13];
- *Traumatic events:* in some cases, the detachment of the retina is consequent to an injury to the face or eyeball associated, for example, with high-impact sport activities or at high speed;
- *Cataract surgery:* in some cases, retinal detachment is a serious complication of cataract surgery that can occur in the early or postoperative periods [13].

Depending on the pathogenesis, three types of retinal detachment can be distinguished. They are schematized in Figure 6 and described below.

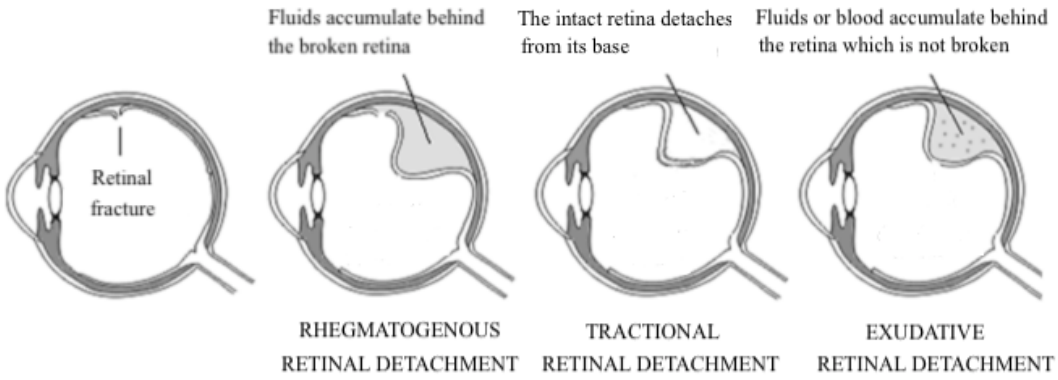

Figure 6 Types of retinal detachment

In the *rhegmatogenous retinal detachment* the initial event consists in the contraction, due to different reasons, of the vitreous body, the transparent fluid that fills the space between the posterior surface of the crystallin lens and the walls of the retina, to which it adheres. This contraction could result in one or more retinal small fractures, due to the presence of pre-existing degenerative areas that make the retina fragile or thin, or lacerations, due to abnormal adhesions and tensile forces. In this way, the vitreous liquid is free to filter into the subretinal space causing the retina to lose adhesion with the pigmented epithelium.

A *tractional retinal detachment* occurs when fibrovascular tissue is formed as a result of trauma, inflammation or neovascularization. This fibrous matrix will pull the sensory retina from the retinal pigment epithelium.

Finally, an *exudative retinal detachment* occurs due to inflammation, injury or vascular abnormalities and results in fluid accumulating in the space below the retina without the presence of a hole or break.

Retinal detachment can be diagnosticated by *ophthalmoscopy*, a technique that uses an instrument that projects a beam of light through the pupil of the eye onto the retina. The

ophthalmoscope provides detailed information about the internal ocular structures and gives the doctor the possibility to see any retinal holes, lacerations or more serous detachments.

1.1.3.2 Treatments

Retinal detachment is treated like a medical emergency, as the risk of sight loss is high. If the intervention is immediate, the risk of permanently losing sight is greatly reduced. In most cases (85 %), only one surgery is needed to successfully reposition the retina and repair the lacerations present. Currently, about 95 % of cases of retinal detachment can be repaired successfully [28]. Unfortunately, after treatment, some patients do not fully recover their vision and may report permanent reduction of central or lateral vision, particularly if the macula was involved in the area of the detachment. Treatment failures usually involve either the failure to recognize all sites of detachment, the formation of new retinal breaks, or proliferative vitreoretinopathy [28].

There are several types of surgical approaches available to treat retinal detachment, including cryopexy and laser photocoagulation, scleral buckle surgery, vitrectomy and pneumatic retinopexy.

Cryopexy and laser photocoagulation are occasionally used alone to restore a small affected area so that the detachment does not spread. Cryosurgery is related to the use of extreme cold surgery in order to destroy abnormal or diseased tissues: its use for the treatment of retinal detachment generates a strong welding of the break margins. Laser photocoagulation works according to the same principle, the difference lies in the medium used which in this case in not a cold liquid or gas but a laser.

The *scleral buckle surgery* is a technique in which the surgeon places one or more silicone bands to the sclera, around the outside of the eye (Figure 7). This allows to the retina to settle again on the posterior wall of the eye: it provides a physical stimulus, pressure, to favor retinal reattachment. Typically, the buckle itself does not prevent a retinal break from opening again. Therefore, in addition to this procedure surgeon typically use laser photocoagulation. The risks for the surgery include infection, a raised pressure inside the eye, bleeding in the eye, detachment of the choroid layer and refractive error.

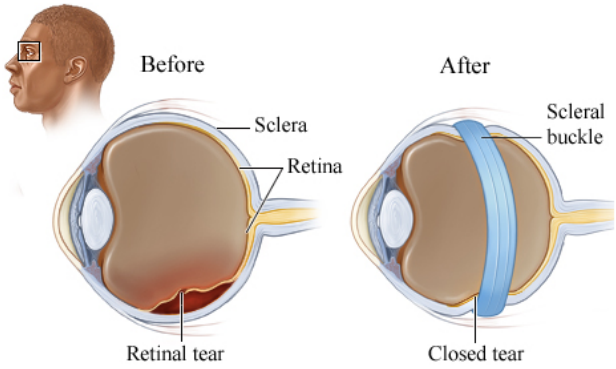

Figure 7 Eyeball before and after the placement of scleral buckle

Vitrectomy is the procedure used in the most complex cases. It consists in the removal of the vitreous gel thus ensuring the complete removal of the vitreous tractions that generated the retinal break. This is replaced by a gas bubble, air or silicone oil (Figure 8). The procedure ends with photocoagulation, to make sure that the retina permanently maintains the correct position.

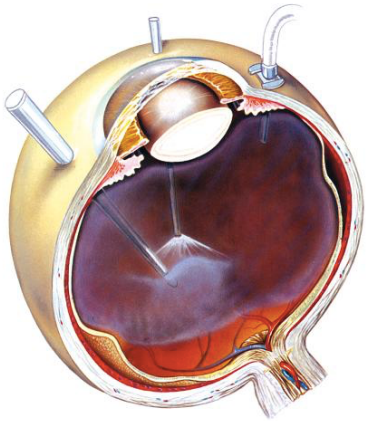

Figure 8 Vitrectomy

The risks associated with vitrectomy are:

- High risk of proliferative vitreo-retinopathy (PVR) in case of failure.
- Retinal detachment occurs again in 3-6% of cases.

When a study compared vitrectomy with scleral buckle surgery, it was found that although there may be less recurrence of detachment, vitrectomy may have little or no difference in success of operation and vision achivied [30]. Both vitrectomy and scleral buckle were associated with side effects: some adverse events appeared to be more common in the vitrectomy group, such as cataract progression and new iatrogenic breaks, whereas others were more commonly seen in the scleral buckling group such as choroidal detachment [30].

The *pneumatic retinopexy* is a technique that can be used if the detachment is mild and easy to repair. It consists in the injection into the eye of a small bubble of gas which will press against the retinal rupture and the surrounding area to seal it. The procedure is followed by photocoagulation to form a scar that helps the retina to fix to the inner wall of the eye. Pneumatic retinopexy has significantly lower success rates compared to scleral buckle surgery and vitrectomy. Initially successful cases have high probability of failing during the weeks and the months after surgery. A study compared outcomes from patients receiving reattachment from pneumatic retinopexy versus scleral buckle. It was found that eyes having received the pneumatic retinopexy procedure were more likely to have a recurrence of retinal detachment by follow-up, and were 11% less likely to achieve retinal reattachment, compared to scleral buckle [12].

The invasiveness of surgical operations and possible complications are the reasons why tissues mechanics is so interest in retina. In fact, this structure is very fragile and knowing its mechanical properties is essential to find a method that can increase the resistance of the retina to mechanical deformation during surgery.

1.2 Mechanical characterization of biological tissues

The study of the mechanical behavior of biological tissues is fundamental not only in the field of tissue and biomedical engineering but also as regards integration with information from sectors such as medicine and pharmaceutical research. Deepening understanding of Biomechanics is aimed at determining the *constitutive link,* i.e the model explaining the mechanical behavior of the tissue *in vivo*.

A *mixed approach* is often used to identify the constitutive link: it allows a partial knowledge of the physical laws that regulate the behavior of the tissue. This approach must follow some essential steps. First of all, an analysis of the composition and the structure of the tissue is required: this can be done with new observations or by referring to the information that can be found in literature. Depending on this first analysis, the context of the constitutive link is chosen, such as elasticity, viscoelasticity, poroelasticity, etc. The next step concerns the execution of experiments, motivated by the chosen field, on samples of biological tissue. Then the *constitutive law* is identified: it is a mathematical equation that describes the experimental behavior of the tissue. Finally, the last two steps concern the determination of the *constitutive parameters*, the coefficients of the constitutive law, and the validation of the model which takes place by comparing the results with the experimental data present in literature.

Dealing with biological soft tissues, it is necessary to take into consideration during the sample experiments some issues such as: non-homogeneity of the tissue and interindividual variability, alteration of the tissue structure during specimen collection, preparation and storage. Major problems also concern the imprecision in the relief of the dimensions of the samples, which are fundamental for the calculation of some parameters, and, finally, difficulties in preparing and grasping the samples. All these issues are true regarding retina tissue. In this work retinal mechanical properties during uniaxial tensile tests were analyzed.

1.2.1 Uniaxial tensile test

The uniaxial tensile test consists in applying a known axial tensile stress, force or elongation, to the test specimen, measuring its response in terms of axial elongation or stress. The test process involves placing the specimen between two grips, as shown in Figure 9, and slowly pulling it until fracture to establish how easily the sample deforms and breaks. In our case, a travel ramp has been applied to the upper grip with a speed equal to 0.1 mm/s which can be described by the relationship:

$$v = \varepsilon_0 \frac{L_0}{t_0} \quad [mm/s]$$

Where ε_0 is the constant deformation imposed, t_0 is the time at which it is reached and L_0 is the initial length of the sample.

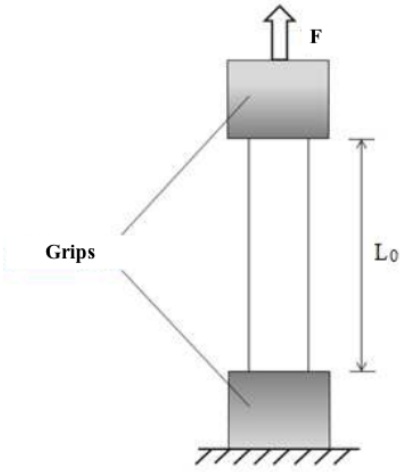

Figure 9 Scheme of a tensile test

Starting from the information obtained by the test, it is possible to calculate the main mechanical characteristics of the material thanks to De Saint Venant's theory of solids. In particular, in this project, some parameters were of fundamental importance, and will be reported below.

The *engineering strain* ε can be calculate using the following relation:

$$\varepsilon = \frac{\Delta L - L_0}{L_0} = \frac{L - L_0}{L_0} \quad [mm/mm]$$

Where ΔL is the change in the sample length, L_0 is the initial length and L is the final length. In the case of a time dependent tensile test the strain is calculated as:

$$\varepsilon(t) = \frac{L(t_i) - L(t_{i-1})}{L_0} \quad [mm/mm]$$

Where $L(t_i)$ is the length at the time *i,* $L(t_{i-1})$ is the length at the time *i-1* and L_0 is the initial length.

The force measurement is used to calculate the *engineering stress* σ*:*

$$\sigma = \frac{F}{A} \quad [Pa]$$

Where F is the tensile force and A is the nominal cross-section of the specimen. In the case of a time dependent tensile test the stress is calculated as:

$$\sigma(t) = \frac{F(t) - F_0}{A_0} \quad [Pa]$$

Where F_0 is the tensile force at time zero, $F(t)$ is the tensile force at time t and A_0 is the nominal cross-section of the specimen.

If stresses and strains are known for each moment of the test, it is possible to obtain a stress-strain curve which, in the case of viscoelastic materials, to which the retina belongs as found in literature, has the shape shown in Figure 10.

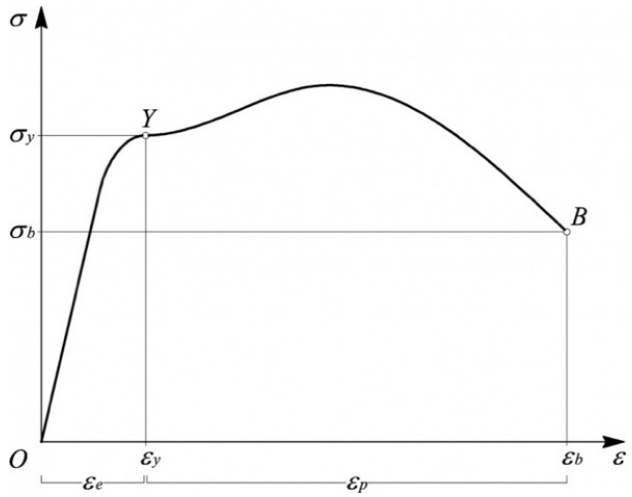

Figure 10 Example of stress-strain curve

During every tensile test the viscoelastic sample passes through different phases which can be identified within the stress-strain diagram:

- The *elastic field* (0-Y) corresponds to the first phase of elastic linear deformation of the specimen. Deformations that occur in this phase are reversible and so, by removing the force there are no residual deformations of the sample but its initial length is restored.
- The end of the elastic field is determined by the *yield point* (σ_y): it determines a reduction in the strength of the material due to micro-cracks inside it. From this point the plastic field starts.
- In the *plastic field* (Y-B), the deformations are irreversible, which implies that, removing the load or the force, the sample shows residual deformations and therefore the deformations are no longer reversible.
- Once the maximum point of the graph has been reached, continuing the test leads to the breaking point (B). At this point corresponds the tensile failure stress (σ_b).

Knowing the stress and the strain it is also possible to calculate other characteristic properties of the material. In particular for our study a central role has been covered by the *Young's modulus (E)* which can be calculated through Hook's law as:

$$E = \frac{\sigma}{\varepsilon} \quad [Pa]$$

E is a mechanical property that measures the stiffness of a solid material, the greater its value the greater the stiffness of the material. It defines the relationship between stress and strain in a material in the linear elasticity regime of a uniaxial deformation. In the stress-strain diagram corresponds to the angular coefficient of the linear section which represents the elastic field.

Chapter 2: State of the art

Only few studies have examined the mechanical properties of the retina [2]. In fact, since retina is so fragile as a biological material, its mechanical behavior has not received serious attention [26]. Although knowing mechanical properties is fundamental for many reasons, such as building reliable tissue engineered retina models.

This chapter aims at introducing the state of the art of the knowledge of retinal mechanical behavior through three previous studies, which will then be compared with the results deriving from this work.

In all the three works considered, as well as in the present, porcine retina was used in order to evaluate the mechanical properties of the retina. This is because, as it can be seen in Table 1, the pig eye is dimensionally and structurally similar to the human one compared to that of other species and is also easily available. The main difference between porcine and human retina is the absence of fovea and macula in the pig, however this is not relevant for mechanical properties. Figure 11 shows a schematic comparison between human and porcine retina.
The wording “tapetum”, in Table 1, refers to a reflective layer placed immediately behind the retina of some animals. Its task of reflecting light towards the retina increases the amount of light that can be captured by the retina itself and its absence is another common point between the human eye and the pig one.

Species	Axial length [mm]	Cornea thickness [mm]	Macula	Fovea	Tapetum	Retina thickness [mm]
Human	23	0.5	Yes	Yes	No	0.1-0.4
Pig	24	1	No	No	No	0.3-0.4

Table 1 Comparison between the human and the pig eye

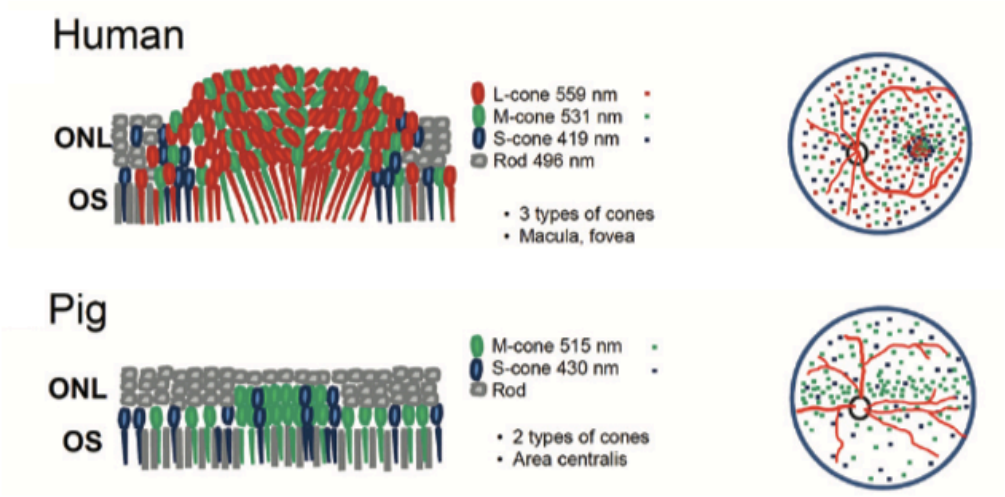

Figure 11 Schematic representation of the human and the porcine retina. The sign "ONL" stays for Outer Nuclear Layer while the sign "OS" stays for Outer Segment

2.1 Biomechanical characteristics of retina

In 2004 Gregor Wollensak and Eberhard Spoerl, of the CGC University's Department of Ophthalmology in Dresen, Germany, published a study whose aim was to examine the biomedical properties of porcine retina [25].

The samples were taken from enucleated porcine eyes within six hours postmortem and the average age of pigs was four months. The retina strips obtained had a length of 10 mm and a width of 7 mm and had been cutting paying attention to exclude the main vessels. The thickness was measured histologically and was found to be 0.252 ± 0.018 mm. After that, the specimens were transferred to a biomaterial test machine (MINIMAT, Rheometric Scientific GmbH) with a distance of 6 mm between the grips, as shown in Figure 12.

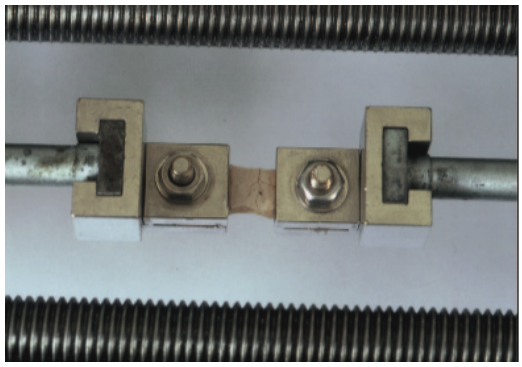

Figure 12 Biomaterial tester with clamped porcine retina [25]

For stress-strain measurement 10 retina strips have been subjected to traction until failure with a velocity of 0.03 mm/s while 10 with a speed of 1.65 mm/s.
Figure 13 and Table 2 show the stress-strain curves corresponding to both test conditions and the main mechanical parameters measured respectively.

The study suggested that the biomechanical behavior of the retina is characterized by a short elastic phase and a remarkably broad plastic phase [25] which becomes shorter with a higher strain rate. However, the strain rate seemed not to affect the initial linear phase.

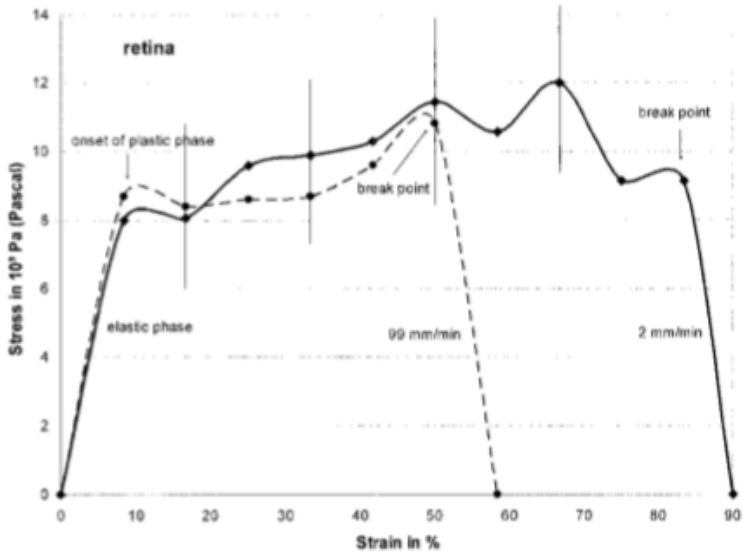

Figure 13 Stress-strain curves of retina with 0.03 mm/s and 1.65 mm/s (dashed lines) strain rate [25]. On x-axis the strain [%] while on y-axis the stress [10^3 Pa]

Parameters	Retina 0.03 mm/s (n=10)	Retina 1.65 mm/s (n=10)
Young's elastic modulus [kPa]	100	110
Stress at break point [kPa]	9.2 ± 1.4	11.3 ± 2.2
Yield stress [kPa]	8.0 ± 2.1	8.2 ± 1.4
Range of Plastic Phase Strain [mm/mm]	0.735 ± 0.022	0.422 ± 0.041

Table 2 Biomechanical parameters [25]

2.2 Dependence of the mechanical properties of the retina on temperature

Chen and Weiland in 2012 studied the relationship between the mechanical properties of porcine retina samples and temperature during the tensile tests: equal amount of samples (n=5) were tested at body temperature (37.0 ± 0.3°C), room temperature (26.1 ± 0.1°C) and low temperature (7.8 ± 1.2°C) [3].
The 15 eyes they used were obtained within 3 hours postmortem and belonged to pigs aged between 3 and 7 months.
A retina flap of 1.5 mm in length and width and 0.3 ± 0.07 mm in thickness was taken from each eye: the sample was first immersed in a saline solution for 5 minutes and then remained in the saline when it was deformed by the tensile machine (Bose Electroforce 3100) with a displacement applied at 1mm/s [3]. The saline temperature was controlled through a heating system, part of the machine, and a chiller.

Figure 14 shows the stress-strain curves obtained in the three different test conditions while Table 3 lists the mechanical parameters of the tissue obtained by the study. In particular, they found out that the retina at 26.1 ± 0.1°C and 7.8 ± 1.2°C is significantly stiffer than the retina at 37.0 ± 0.3°C. Moreover, the retina at 7.8 ± 1.2°C is slightly stiffer than the retina at 26.1 ± 0.1°C, but the difference is not significant. As for the trends of the curves they seem to confirm the results obtained by Wollensak. In fact, also in this case, the curves are characterized by a linear elastic phase followed by a plastic region.

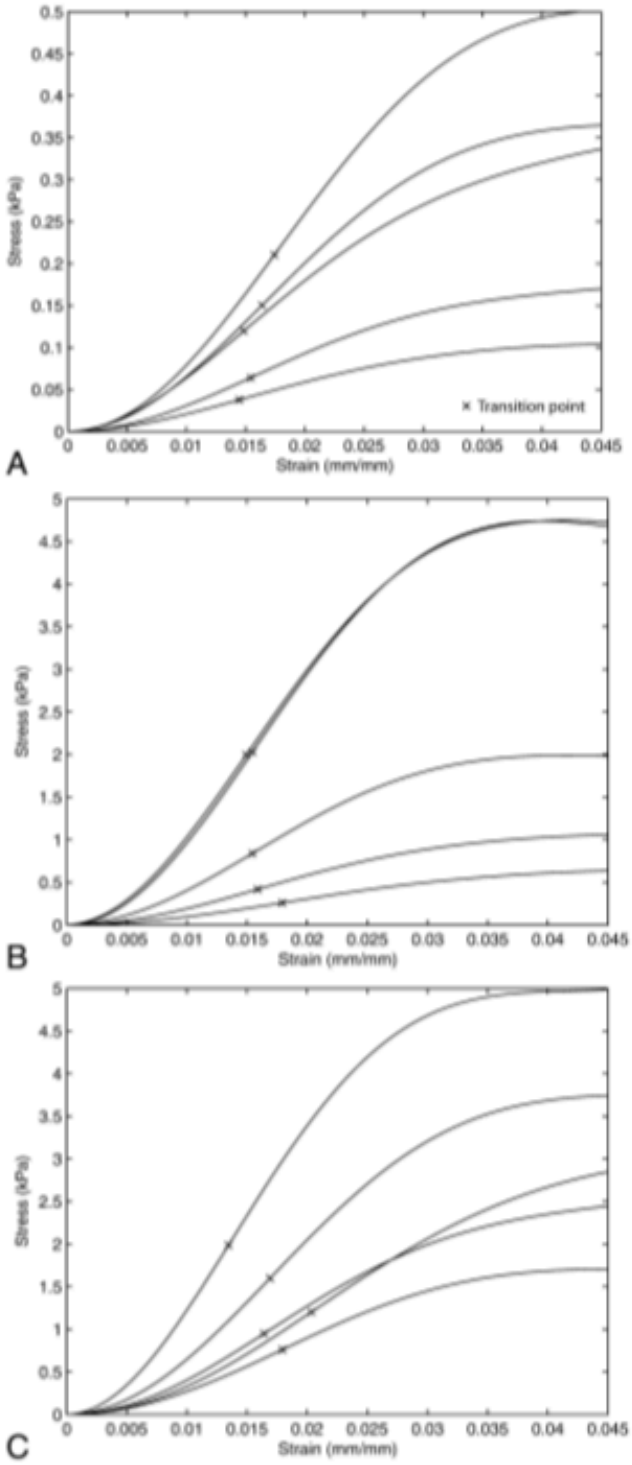

Figure 14 Stress-strain curves of the porcine retinal strips at (a) body temperature (37.0 ± 0.3°C), (b) room temperature (26.1 ± 0.1°C) and low temperature (7.8 ± 1.2°C) saline [3]. Stress is expressed in [kPa] while strain in [mm/mm]

Parameters	37.0 ± 0.3°C (n=5)	26.1 ± 0.1°C (n=5)	7.8 ± 1.2°C (n=5)
Transition modulus [kPa]	11.2 ± 6.10	111.25 ± 88.16	125.13 ± 63.61
Transition stress [kPa]	0.12 ± 0.07	1.11 ± 0.85	1.30 ± 0.50
Transition strain [mm/mm]	0.016 ± 0.001	0.016 ± 0.001	0.017 ± 0.003

Table 3 Biomechanical parameters [3]

2.3 Contribution of blood vessels to the mechanical properties of retina

Chen and Weiland, in 2010, studied the dependence between the mechanical behavior of the tissue and the presence of vessels in different directions, assuming that the retina should be treated as an anisotropic and inhomogeneous material from a mechanical point of view [2].

They used 10 porcine eyes obtained 3 hours postmortem belonging to animals which age is unknown. To examine different vessel types and sizes, 3 strips of retinal samples were dissected in each of 5 pig eyes: one strip contained the superior-temporal vein in the axial direction, one strip contained the superior-temporal artery in the axial direction and one strip did not contain any visible vessels. To examine different vessel orientations 2 strips of retinal samples were dissected in each of 5 other pig eyes: one strip contained the superior-temporal vein in the axial direction and one strip contained the superior-temporal vein in the circumferential direction. [2]. As regards the dimensions, the samples were characterized by a length and width of 1.5 mm and a thickness of 0.3 ± 0.08 mm. Strips were transferred to the tensile machine (Bose Electroforce 3100) and subjected to a displacement applied at 1 mm/s until fracture.

Figure 15 shows an example of the five possible of stress-strain relationship of the retinal strips that contained the superior temporal vein, the superior temporal artery or did not contain any visible vessels, while Table 4 shows the different values of the biomechanical parameters in the three mentioned conditions.
The obtained results establish that the dimension or absence of vessels significantly influence the parameters of interest, in particular the Young's modulus.

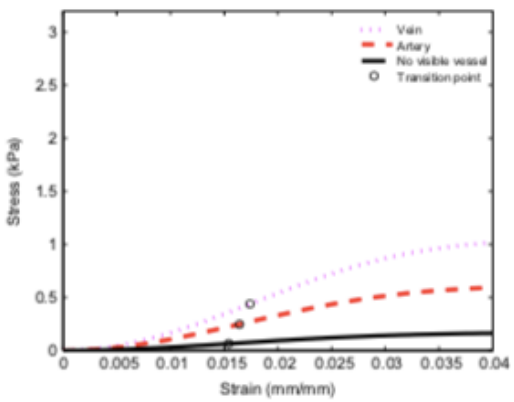

Figure 15 Stress-strain curves of strips containing superior-temporal vein (pink), superior-temporal artery (red) and no visible vessels (dark) [2]. Stress is expressed in [kPa] while strain in [mm/mm]

Parameters	Vein	Artery	No visible vessels
Transition modulus [kPa]	50.90 ± 42.39	38.48 ± 16.64	11.12 ± 6.10
Transition stress [kPa]	0.57 ± 0.47	0.41 ± 0.18	0.12 ± 0.07
Transition strain [mm/mm]	0.018 ± 0.002	0.016 ± 0.001	0.016 ± 0.001

Table 4 Biomechanical parameters of strips containing vein, artery and no visible vessels [2]

Concerning vessel orientations, Figure 16 shows an example of stress-strain curves of strips that contained the superior-temporal vein in the axial and in the circumferential directions. Instead, Table 5 shows the values of the biomechanical parameters in the two considered test conditions.

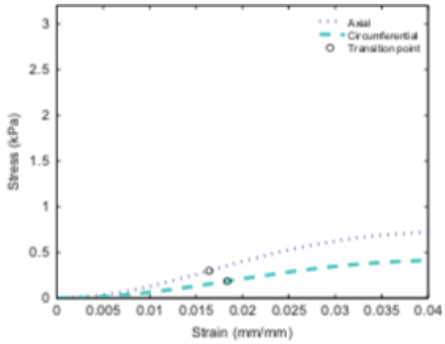

Figure 16 Stress-strain relationship of retinal strips containing the superior-temporal vein in the axial (lilac) and circumferential (green) directions [2]. Stress is expressed in [kPa] while strain in [mm/mm]

Parameters	Axial direction	Circumferential direction
Transition modulus [kPa]	47.58 ± 27.16	24.67 ± 11.88
Transition stress [kPa]	0.49 ± 0.27	0.27 ± 0.12
Transition strain [mm/mm]	0.016 ± 0.001	0.018 ± 0.002

Table 5 Biomechanical parameters of strips containing vein in axial and circumferential directions [2]

Chen and Weiland found that retinal blood vessels contribute significantly to the stiffness of the tissue, and the size of the vessels is the only determining factor [2]. In fact, if the dimension of the vessels or their absence determine a significant change in the stiffness of the retinal samples, considering different orientations of blood vessels, there is no significant evidence to prove that they affect the mechanical properties of the retina. Finally, the shapes of the curves seem to confirm the results of the two previous studies.

Chapter 3: Materials and methods

As previously mentioned, the aim of this thesis project is to analyze the retina from a biomechanical point of view by performing uniaxial tensile tests with consequent calculation of some fundamental mechanical parameters. This need arises from the fact that, over the years, the mechanical behavior of the retina has not been fully investigated due to its structural fragility. However, the knowledge of the mechanical properties of such a delicate tissue represents the starting point for some considerations regarding, for example, the improvement of pre-existing surgical techniques or the development of in vitro and in silico models that can describe the behavior of the retina at a given stimulus.

In this chapter the procedures and details relating to the tensile tests performed will be explained. The samples were extracted from pig eyes, supplied by *Fumagalli Industria Alimentari Spa (Tavernerio, Como),* and then analyzed within at most 10 hours of the animal's death at *LaBS, Department of Chemistry, Materials and Chemical Engineering (Milan Polytechnic).* The tests were carried out, at first, with a tensile machine (TC3F, EBERS) on two types of samples: the former includes the retina and the optic nerve, which was then used as a gripping, the latter consists in the folding of the retinal tissue into a known number of layers. Moreover, in this last case, the tests were performed in presence of Saline Phosphate Buffer (PBS) (Sigma).

Moreover, the tensile tests on the retina without optic were also performed using another testing machine (EnduraTEC ELF 3200, BOSE), with the aim of comparing data deriving from two different types of machines.

Finally, an additional analysis of this thesis project was the one concerning the initial calculation of the deformation fields of the retina samples through the *Digital Image Correlation* (DIC), an optical analysis for accurate 2D and 3D measurements which will subsequently be illustrated in detail.

3.1 Samples collection and preparation

Regarding the preparation of the samples, we have to distinguish between retina with and without the optic nerve. In particular, the first stages of the preparation are the same for both samples, the difference lies in the final step, i.e. the extraction of the specimen from the eyeball.

3.1.1 Retina with optic nerve

The extraction of a fragile tissue such as the retina is an extremely delicate and complex operation. In fact, it appears to be firmly anchored near its outermost layer to the sclera and near the innermost layer to the vitreous body. For this reason, at first, we hypothesized that the best way to preserve most of the tissue, without damaging it, was to leave it attached to the optic nerve. Figure 17 shows the main steps of the extraction of this type of sample, in order from left to right.

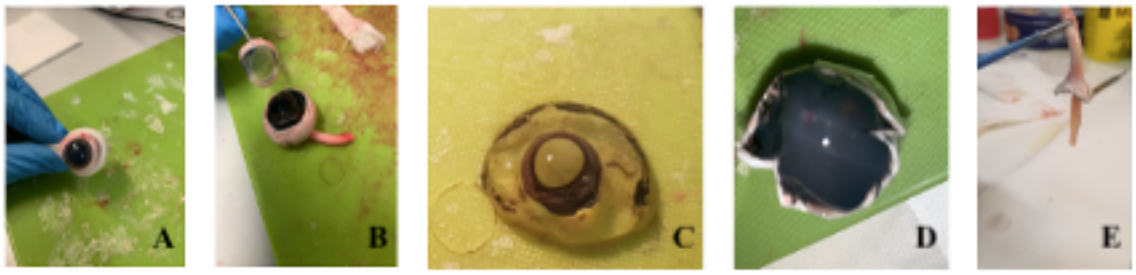

Figure 17 Extraction of the retina attached to the optic nerve

After cleaning the eyeball from excess skin, the eyeball was wrapped with a strip of sterile gauze so that the sclera remained tight (Figure 17A). Then, with a surgical scalpel, the eyeball was incised at a slightly higher level than the equatorial one. In this way it was possible to remove the cornea (Figure 17B) and, subsequently the vitreous body (Figure 17C), taking care that the retina did not remain attached to it. At this point the retina, which appears opaque white in Figure 17D, was attached only to the sclera. With the help of a small spatula, or tweezers, the retina was delicately detached from the sclera and gradually the sclera was cut through the use of a pair of surgical scissors. At the end of the operation, the

retina remained attached almost only to the optic nerve (Figure 17E) and was placed in a petri dish containing PBS, so that it remained hydrated until the time of the test.

3.1.2 Retina without optic nerve

The major problem with specimens attached to the optic nerve is the measurement of thickness. In fact, what is obtained is a packing of tissue in which it is not known how many times the retina is folded on itself. From this problem arose the second extraction protocol: if we were able to extract a single retina sheet and fold it on itself a known number of times, in our case two or four, knowing the thickness of the single sheet we could have estimated the thickness of the sample more precisely. Figure 18 shows the extraction protocol for this type of specimen.

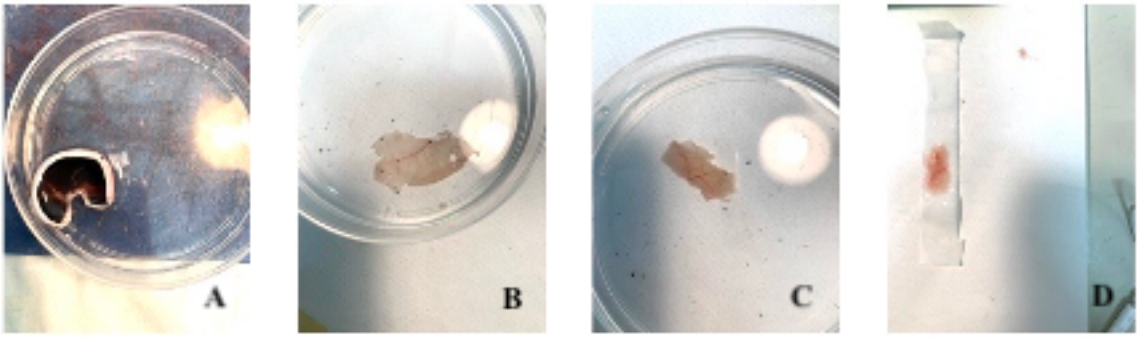

Figure 18 Extraction of the retina without optic nerve

The initial steps for extraction are the same as for specimens attached to the optic nerve (3.1.1). Once the cornea and the vitreous body were removed, the sclera with the retina still attached was placed in a petri dish filled with PBS (Figure 18A). The presence of this solution facilitated the detachment of the retina from sclera by tweezers. Subsequently, always with the help of tweezers, the single sheet of retina was folded on itself two or four times (Figure 18C), depending on the size of the tissue extracted without visible breaks. Finally, the sample was removed from the PBS with the aid of a strip of baking paper (Figure 18D), the ends of which were then cut. This proved to be a fundamental step for the sample transfer operation on the test machine.

3.2 Optical coherence tomography for the measurement of retinal thickness: working principle and application to the samples

Before performing the tensile tests, some dimensional measurements, fundamental for the calculation of stress and strain, were carried out. In particular, the following were calculated: the initial length (L_0) of the sample, defined as the distance between the grips before the start of the test, its width and its thickness. Regarding the samples attached to the optic nerve the measurement was performed in an approximative way using a digital caliper (Mitutoyo, 150 mm), as shown in Figure 19, as for the width. It was not possible to realize a more precise estimation because, as previously mentioned, what is obtained at the end of the extraction of the sample is a packing of tissue in which it is not known how many times the retina has folded on itself.

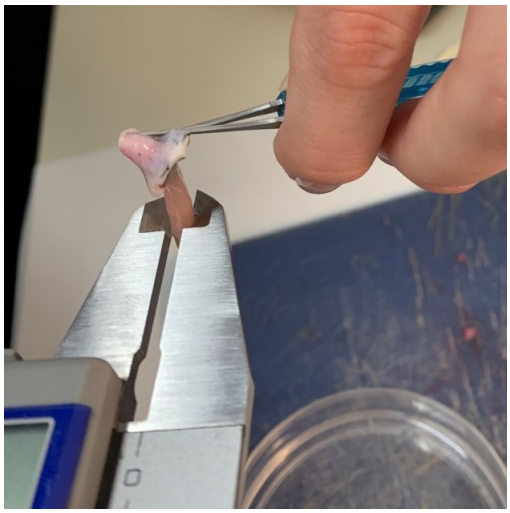

Figure 19 Thickness measurement with digital caliber for samples with optic nerve

On the contrary, it was possible to estimate the thickness of the sample without optic nerve with greater precision. Indeed, by folding the retina specimen a known number of times and knowing the thickness of the initial sheet it was possible to obtain a more truthful measurement. As for the thickness of the single sheet of retina, the measurements were made thanks to the collaboration of Dr. Paolo Arpa at his clinical center using optical coherence tomography (OCT). The OCT is a particularly important technique in ophthalmology as it provides real-time images of cross sections of the retina and the anterior chamber of the eyes,

allowing, not only to evaluate macular pathologies, but also to obtain quantitative measures. This paragraph will summarize the working principle of this technique and subsequently explain how it was applied to our samples.

Optical coherence tomography is a technique that provides high resolution (μm) images of cross sections of biological tissues as shown, for example, in Figure 20. Regarding clinical applications, it is used, for example, as an alternative to excisional biopsy if it proves too risky to perform. It is also used as a guide to the correct localization of the portion of tissue to be extracted during biopsy or to surgical procedure. As said before, the OCT is a technique of particular importance in ophthalmology not only for the evaluation of macular diseases but also for obtaining quantitative measures.

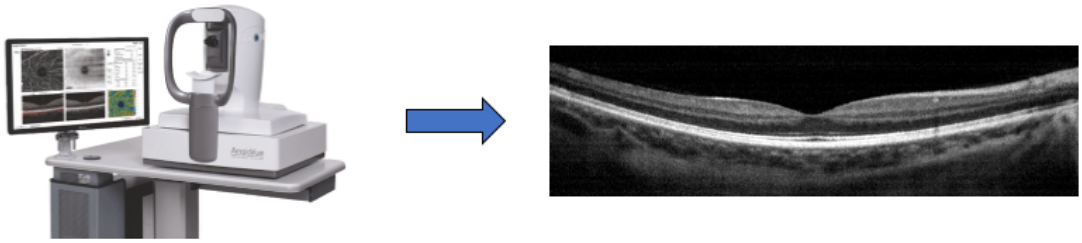

Figure 20 OCT machine and obtained image of the retina tissue

Through the OCT, the distances and the dimensions of the different ocular structures are determined by measuring the delay time of the echo of light that is reflected or backscattered by the different structures as the axial distance. The *temporal resolution* associated with the instrument capable of measuring the delay of the light echo is defined as:

$$\Delta T = \frac{\Delta z}{v} \quad [s]$$

where Δz is the distance traveled by the echo while v is the velocity of propagation of the echo through the tissue.

The OCT exploits the phenomenon of light interferometry. As Figure 21 shows, the OCT light source is divided by a beam splitter into two coherent light beams: one beam is directed

towards a reference (the reference arm in Figure 21), while the other is conveyed towards the sample to be examined, i.e. the tissue eye. Subsequently, the light beams reflected by the reference and the sample interfere and recombine in a single beam that will reach a sensor.

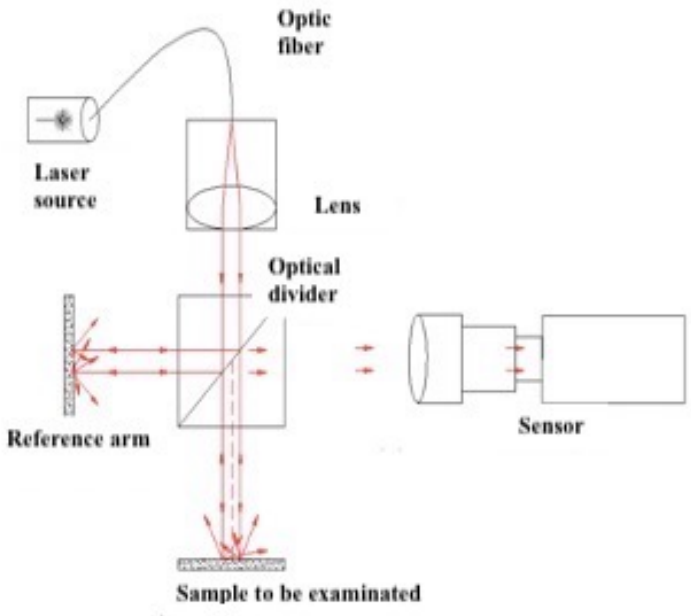

Figure 21 Interferometry operating scheme

Three types of images can be obtained through optical coherence tomography. The first type is represented by the *A-SCAN image:* it is a one-dimensional image in which the data for each point can be represented in a time-amplitude graph of the type shown in Figure 22.

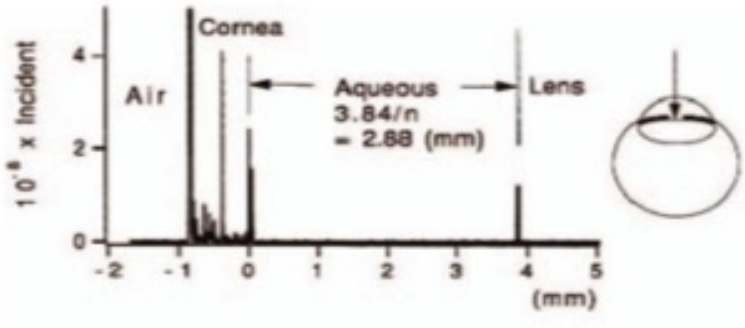

Figure 22 A-SCAN image

The second type of image that we can obtain is the *B-SCAN:* it is a two-dimensional image (Figure 23) obtained by placing side by side about 1600 A-SCAN images performed along a line of about 6 mm in length in the transverse direction. This is the type of image that we used for the evaluation of the thickness of the retina in this thesis project and it is also the one most used in ophthalmology as the images obtained are sections similar to the histological ones. Moreover, they allow the evaluation of the internal structure and, as in our case, the measurement of the thickness.

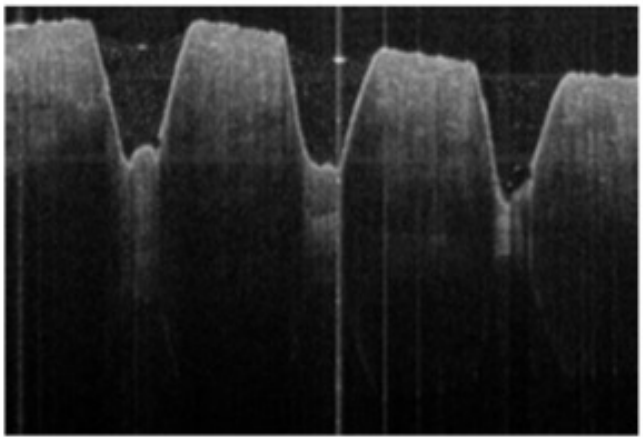

Figure 23 Example of B-SCAN image of the ciliary body

The last type of image that can be obtained is the *C-SCAN* (Figure 24)*:* in this case the image is of a three-dimensional type. This type of image is obtained by placing 256 horizontal B-SCAN side by side and allows to appreciate retinal swellings and any deformations of the retinal surface.

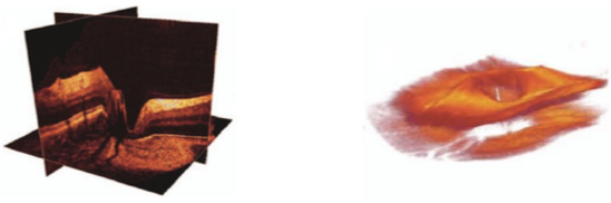

Figure 24 Examples of C-SCAN images obtained with different reconstruction methods

The thickness analysis was carried out on 3 porcine eyes by manually positioning the sample in front of the objective of the optical coherence tomograph (DRI OCT Triton Plus, Topcon), as shown in Figure 25. The type of image obtained is a B-SCAN and the red line associated with a number represents the measure of the retinal thickness (Figure 26).

Figure 25 OCT performed on porcine eye

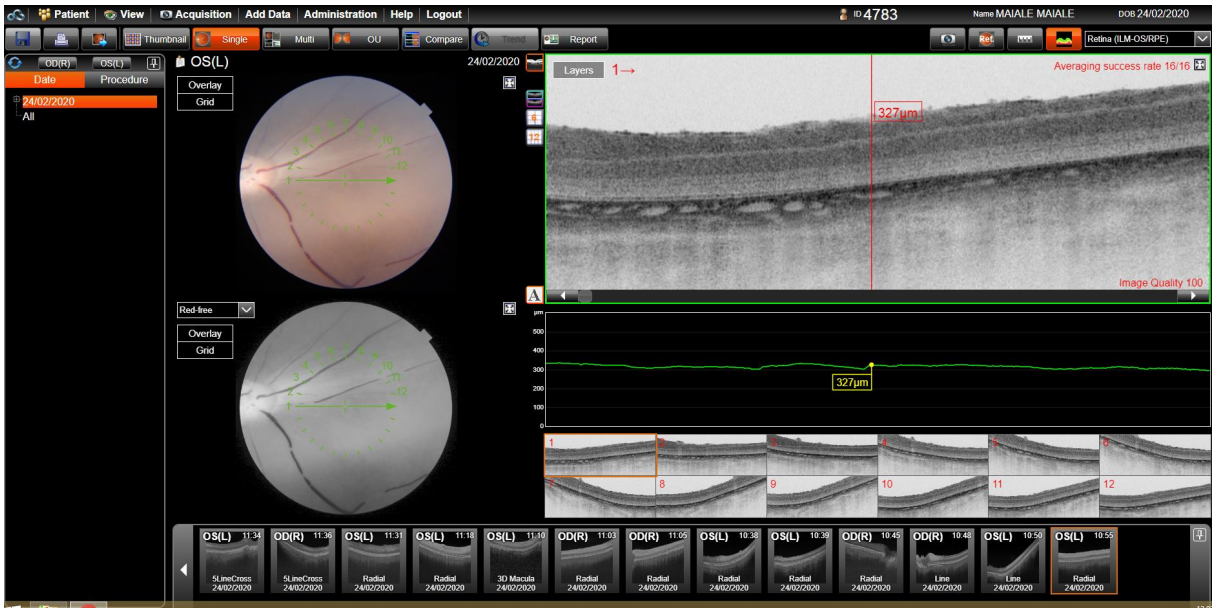

Figure 26 B-SCAN image obtained by the OCT on porcine eye

The three images obtained through OCT were then processed in order to obtain a final average thickness value, as precise as possible, that could be used for all the sample without optic nerve subjected to the tensile test and multiplied two or four times according to the number of folds. The image processing was performed through ImageJ (Figure 27).

The operation was performed, for each of the three tomographic images, in three areas, different from the one considered by the OCT. In this way, four different retinal thickness measurements were obtained for each of the three eyes. For each eye the average value of the four thicknesses was calculated using Excel. Finally, using the three average values obtained, always using Excel, the final average value and the standard deviation were calculated.

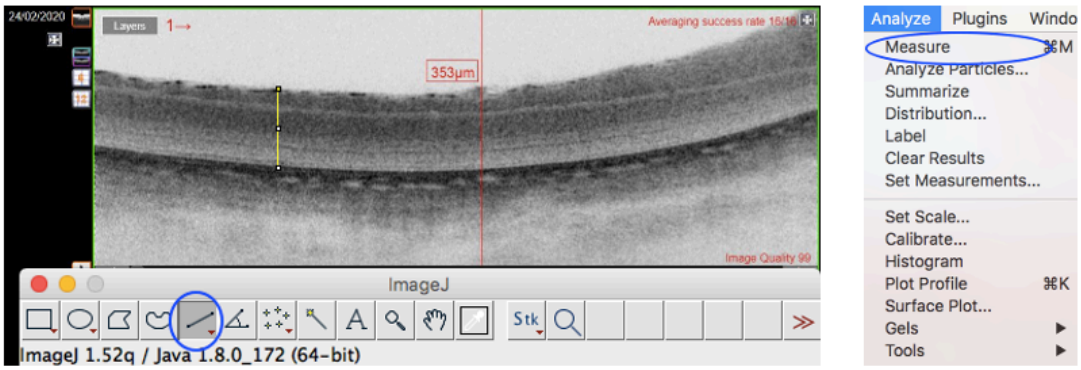

Figure 27 Evaluation of the retinal thickness in different areas

3.3 Experimental mechanical tensile tests

The test procedures for both machines used for tensile testing are shown below. In particular, the general characteristics of the tensile test machines, the sample transfer protocols, and the calculation of the biomechanical parameters are described.

3.3.1 Uniaxial tensile tests performed with TC3F test machine

At first, once the dimensional measurements of the samples were taken, tensile tests were performed using the force measurement machine TC3F shown in Figure 28 (EBERS Medical Technology LS). The main components are the *mechanical actuator*, in the superior part of the machine, that transfer its effect to the sample, the *load cell*, which in our case has a 5 N full scale, and the *test chamber* containing the clamp instrument (Figure 29), which can be disassembled and assembled to facilitate the transfer of the sample between the grips. The maximum distance between the upper mobile grip and the lower fixed grip is 21 mm.

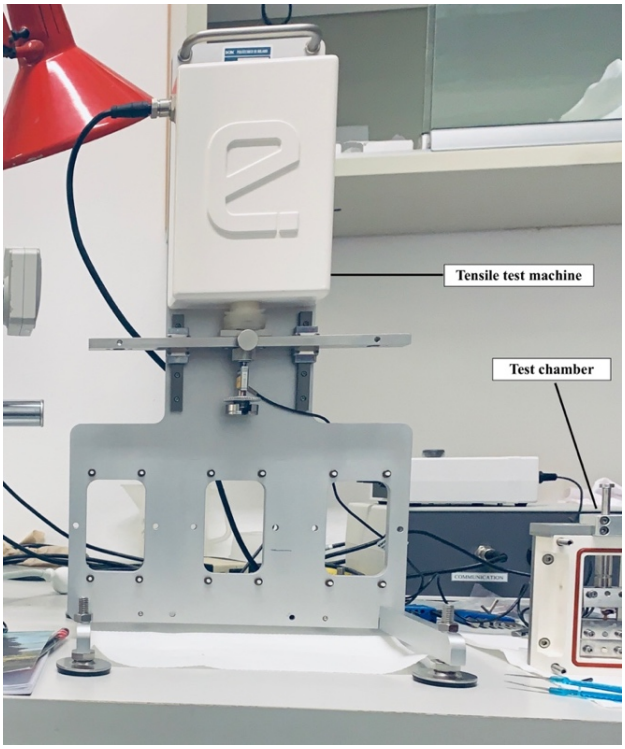

Figure 28 Test machine (TC3F, EBERS) used for tensile tests on retina samples

Figure 29 Test chamber containing the clamp instrument. The upper grip is the mobile one while the lower is fixed

To mount the sample with the optic nerve on the tensile machine, first baking paper was placed on the bases of the two grips to prevent the sample from slipping while clamping (Figure 30A). Then, with the help of tweezers, the sample was positioned between the two bases of the grips with the optic nerve placed on the upper grip. Finally, the sample was fixed by screwing the two clamps to their respective bases, taking care not to include the remaining sclera part in the clamping. At this point, the chamber was mounted on the tensile machine, as shown in Figure 30B where the sample is circled in black.

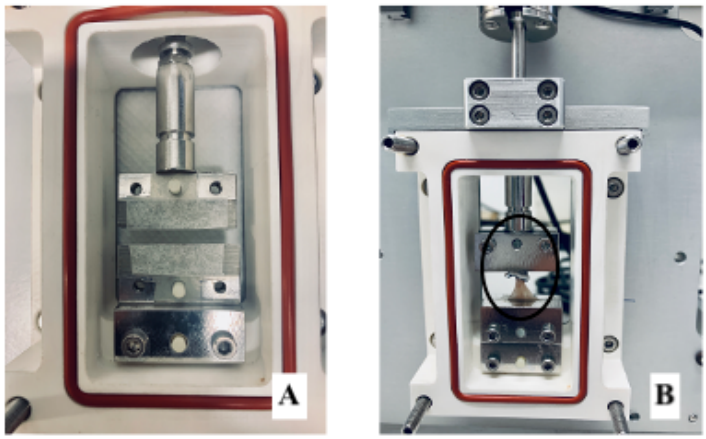

Figure 30 Transfer of the sample with optic nerve into the test chamber

The transfer of the sample without optic nerve is slightly different from the one previously described. Figure 31 shows the main steps of the transfer process of the sample without optic nerve into the test chamber. First of all, the strip of baking paper used to remove the sample from the PBS-filled petri dish, as explained above (3.1.2), was cut at the ends of the obtained tissue (Figure 31A). The paper on which the retina rests was used as a support for the transfer of the sample between the grips. Then, two strips of baking paper were positioned on the bases of the two grips. Subsequently the tissue, attached to the baking paper, was transferred between the grips with the sample in contact with the strips of paper on the metal bases. This was done to prevent the specimen from slipping underneath the grips when placed. Before removing the paper, only one of the two clamps was screwed, generally the upper one. Then, with the help of a syringe filled in PBS, the baking paper was detached from the retina and removed. At this point the lower clamp has also been screwed (Figure 31B). Finally, the test chamber was filled with PBS up to the level shown in Figure 31C and represented by the black line. The chamber was then closed frontally with a plexiglas slide and mounted on the tensile machine.

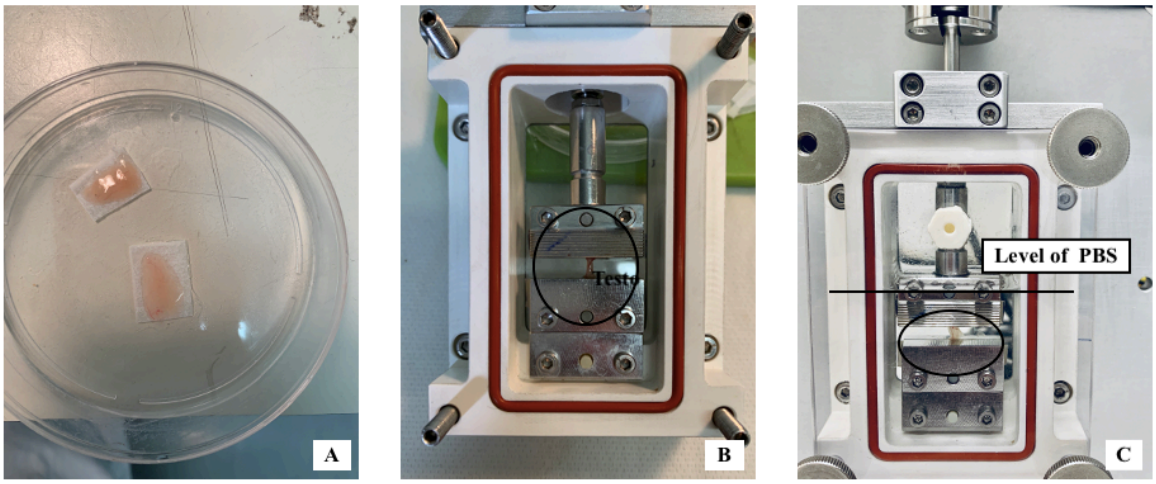

Figure 31 Transfer of the sample without optic nerve into the test chamber

For the mechanical measurements, 9 samples with optic nerve and 9 samples without optic nerve were pulled using the TC3F (EBERS Medical Technology LS) equipped with a 5 N load cell. Regarding the grips the upper one is mobile while the lower one is fixed. Excluding the presence of PBS during tests on samples without optic nerve, the test procedure was the same for the two different types of specimen.

Regarding the setting of the parameters, in our case a travel ramp with a known speed has been applied to the upper grip. The speed and the distance to be traveled are set in the section *velocity mode*. Under the wording "velocity" the desired speed is set, in our case 0.1 mm/s. The travel ramp is set under the heading "travel" and depends on the value of the initial length L_0 as the maximum distance between the grips is 21 mm. For an L_0 = 5 mm, for example, the maximum travel that can be set is 16 mm. The number of cycles has been set to 1, which includes the traction of the sample up to the set distance and its return to the starting point of the test. After setting all the parameters, the test can be started.

At the end of the test the software returns a text file as shown, for example in Figure 32. The upper part shows the information relating to the sample. As far as the columns below we are interested in the first three: the first shows the time (s), the second the displacement (mm) and the third the force applied (N) by the machine. These data were used for the calculation of the biomechanical parameters of the retina sample under examination.

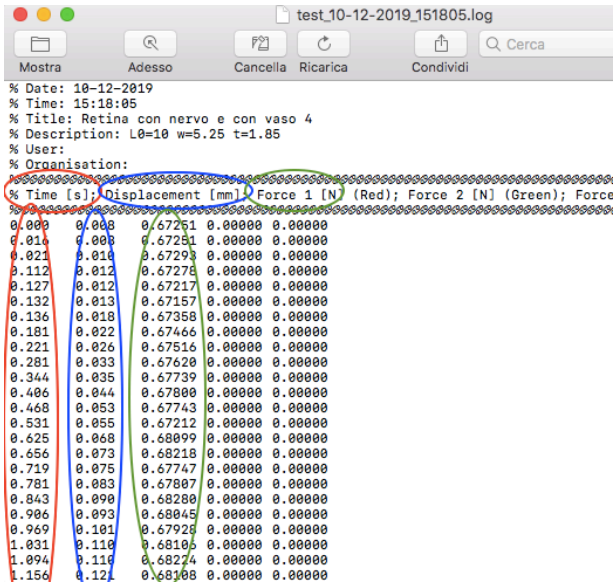

Figure 32 Parameters returned by the software

3.3.2 Uniaxial tensile tests performed with EnduraTEC test machine

Tensile tests were also performed on samples without optic nerve with a second tensile machine (EnduraTEC ELF 3200, BOSE), shown in Figure 33. In this way it was possible to compare results deriving from two different tests protocols as regards this type of samples.

The main components of this single-axis electromagnetic actuation machine, used to perform the tests are the *mechanical actuator*, the *displacement transducer*, LVDT *(Linear Variable Displacement Transducer)* and the *load cell*. The mechanical actuator is located in the upper part of the machine and its effect is transferred to the sample through the upper grip of the clamp instrument for a maximum stroke of 12mm. The displacement transducer allows to measure the displacement applied by the actuator while, the load cell, which in our case has a 22 N full scale, is located in the lower area of the machine and measures the force exerted by the system. Finally, the measured signals are acquired by the machine control unit and sent to the electronic calculator. The interface software between the operator and computer is the *Wintest Digital Control System* which allows to carry out different types of tests by creating the protocol of interest.

Figure 33 Tensile machine EnduraTEC (BOSE)

The test consisted in applying a known travel ramp to the upper grip at a certain velocity. Figure 34 shows a detail of the clamps of the machine on which the samples are transferred before the starting of the tests. In particular, there are two grips: the upper is the mobile one and is mounted integral with the actuator using four mordent screws, while the lower is the fixed one.

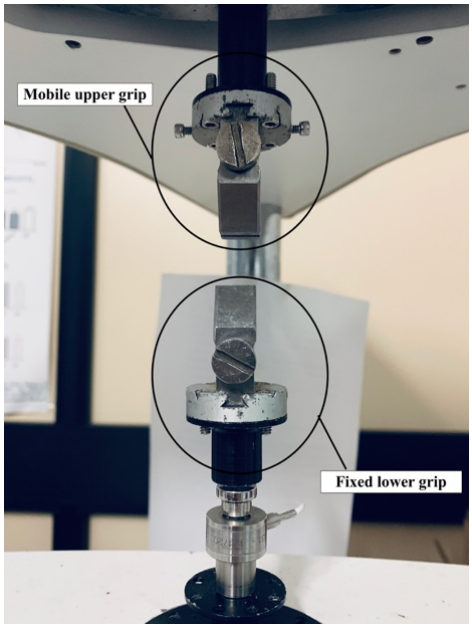

Figure 34 Clamp instrument of the EnduraTEC tensile machine

After the sample was extracted (Figure 35), it can be mounted on the clamp instrument as shown in Figure 36. The baking paper previously used to collect the sample was cut at the ends and was used as a support for the transfer procedure. The retina was first clamped with the upper grip and then was detached from the paper with the aid of a small spatula or tweezers. Then, it was subsequently clamped by the lower grip which was then moved manually downwards so that the sample was well under tension before the start of the test.

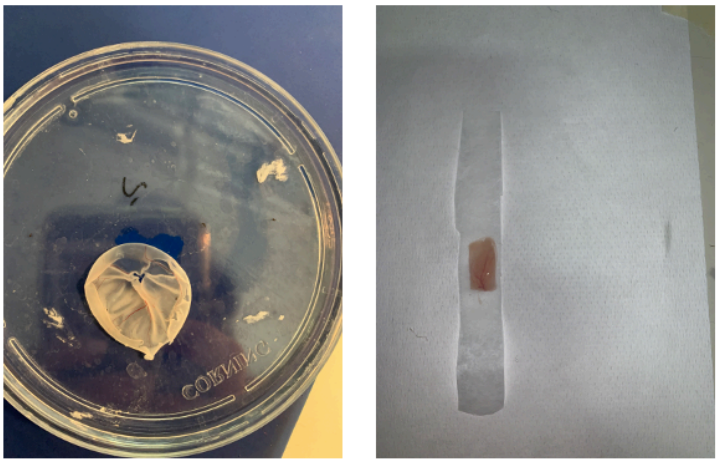

Figure 35 Extraction of the sample without optic nerve

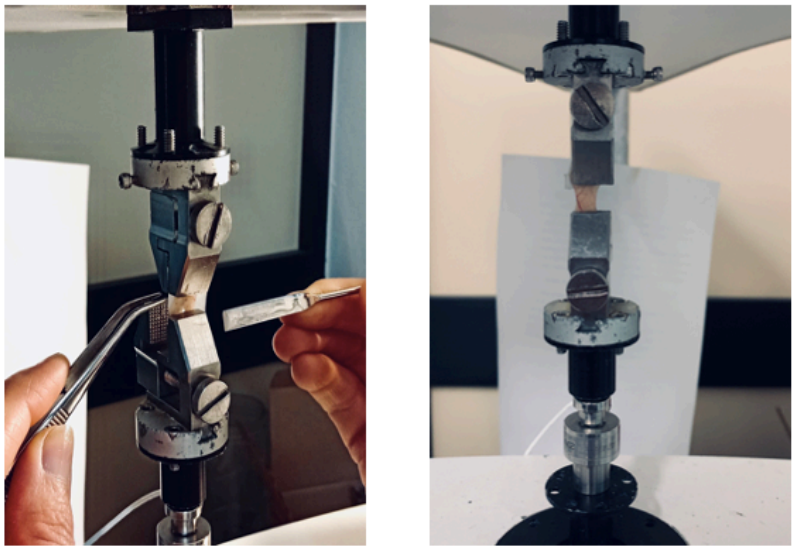

Figure 36 Transfer procedure of the sample to the clamp instrument

Once the sample was transferred between the two grips it was possible to perform the tensile test. Tests were performed on 16 samples without optic nerve and the major difference in comparison with the tests performed with the TC3F machine was the absence of PBS during the proof due to the lack of an adequate chamber test.

The control software through which the experimental tests are programmed is *Wintest Digital Control System* (Figure 37). The window circled in red in the Figure 37 corresponds to the position of the mobile grip, variable between -6 mm and +6 mm, while the window circled in yellow returns the value of the force measured by the load cell.

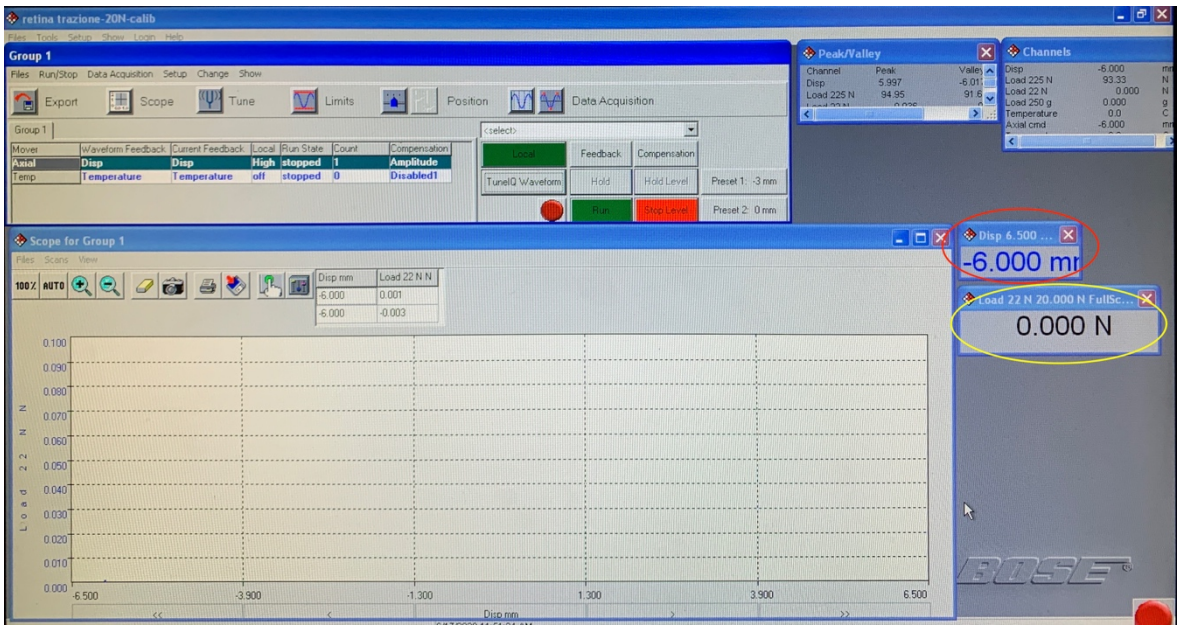

Figure 37 Graphic interface of the Wintest Digital Control System

Regarding the setting of the test parameters, the first thing to do is to move the mobile grip to the position from which you want to start the test. This is possible by clicking on the *Position* button, circled in red in Figure 38, and manually setting the position from the appropriate window.

In our case the upper grip starts its run from -6mm position. It is important to specify that this operation was carried out before the sample was transferred between the grips since moving the upper piston with the retina sample already mounted would have led to its inevitable destruction.

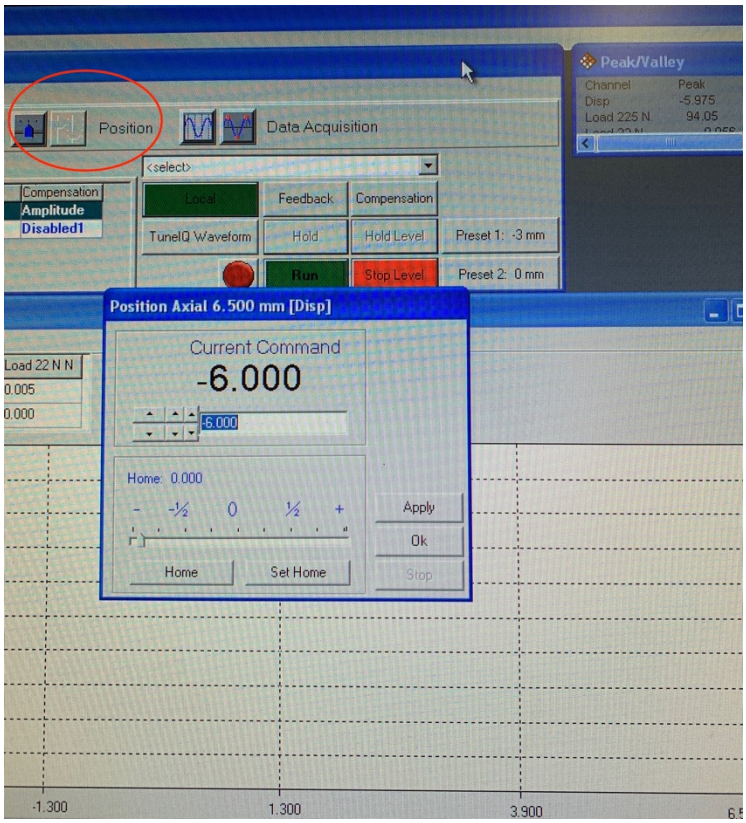

Figure 38 Setting of the initial position of the upper grip

Once the initial position has been set, the sample is mounted between the grips as described at the beginning of this paragraph. At this point, the travel ramp and the displacement velocity were set by clicking on the command *TunelQ Waveform*, circled in red in Figure 39, which subsequently opened the window shown in Figure 40. As regards our tests, the upper mobile grip moves from the -6 mm position to the +6 mm position with a velocity of 0.1 mm/s and the returns to the start position with a speed of 1mm/s. Subsequently, the dimensional measurements useful for calculating the biomechanical parameters of the sample were carried out. Once this is done, the test is started.

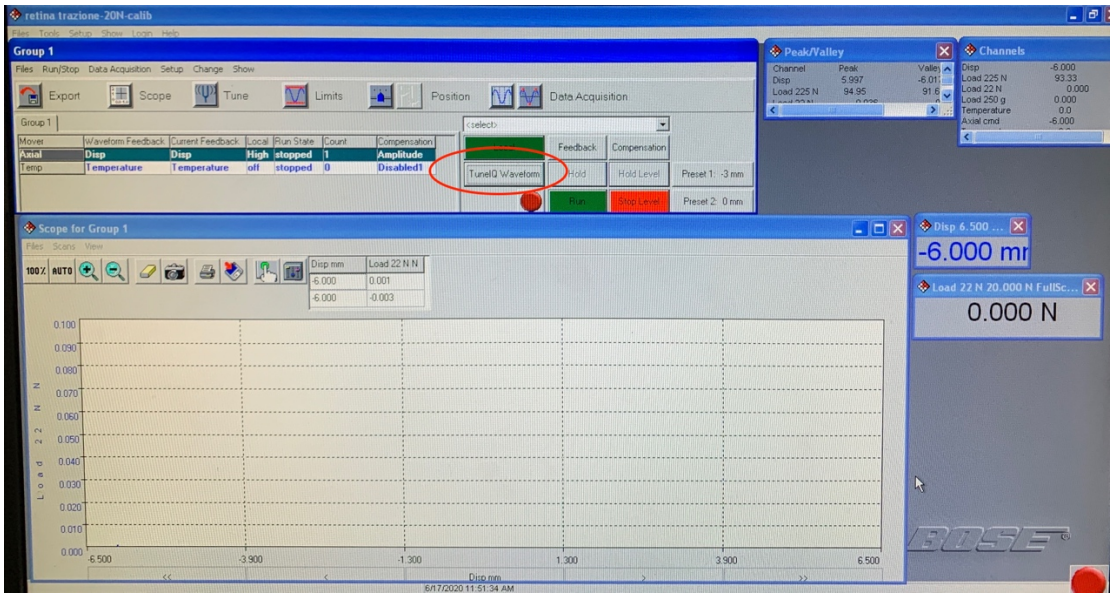

Figure 39 Position of the TunelQ Waveform command

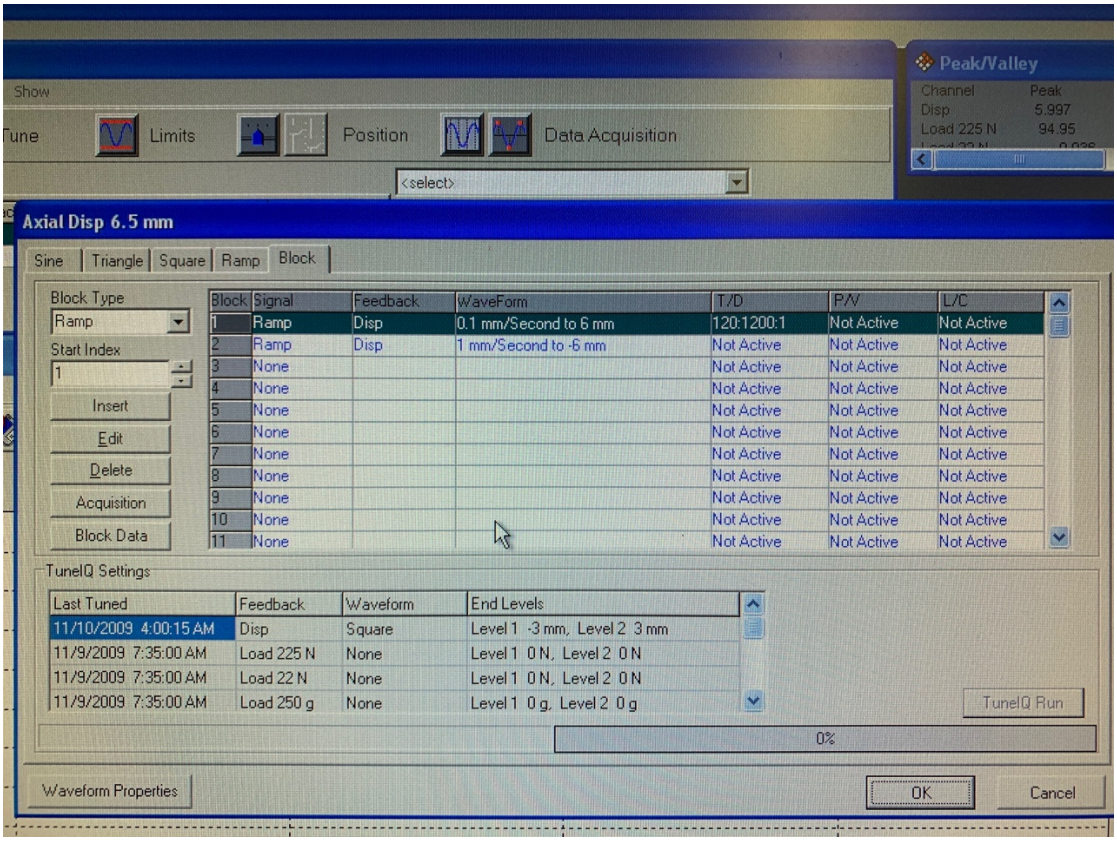

Figure 40 Window for setting the parameters

Once the test is completed, the software returns a text file containing a series of data calculated for each instant of the tensile test, as shown in Figure 41. The first column, circled in red, is related to the time (s), the second represents the displacement (mm) and the third returns the applied force (N).

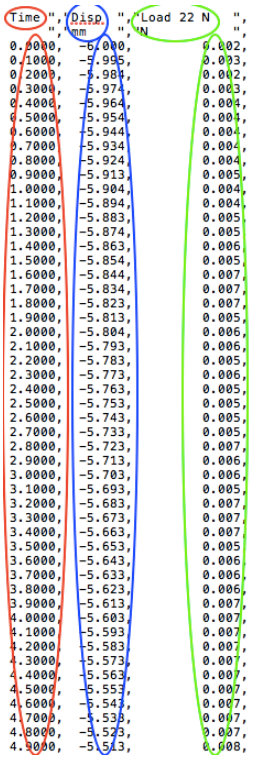

Figure 41 Data returned by the software at the end of the test

3.3.2.1 Design of a chamber suitable for the retina for carrying out wet tests on EnduraTEC test machine

In the case of the tensile tests performed with the EnduraTEC machine, it was not possible to carry out wet tests due to the lack of a suitable chamber for the retina. Although this was not a fundamental requirement for our tests, as the sample after being extracted was immediately transferred to the machine without having time to dehydrate, for one of the final step of this project we concentrated on designing a chamber suitable for the tissue under analysis, so that tests could be carried out in physiological conditions in the future.

Before describing the designed test chamber, I would like to briefly mention the pre-existing one so that the reason that made it unsuitable for our case should be clearer (Figure 42). The test chamber must be mounted on the lower fixed grip. What prevented the transfer of our retina sample between the grips was the fact that this structure has only one mobile side, the front one, while for our transfer protocol (paragraph 3.4.1) it is essential to also have the left and the right sides open. For this reason, a structure has been designed consisting of two assembled pieces which allows the front side and the two lateral sides to be partially free so as not to hinder the transfer of the retina sample between the two grips.

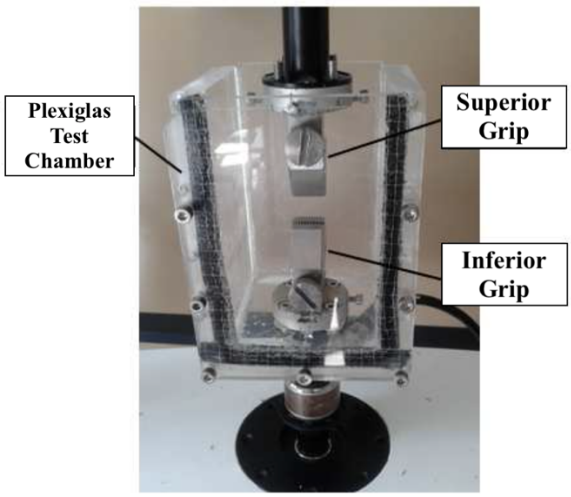

Figure 42 Pre-existing test chamber

A 3D drawing of the designed test chamber is shown in Figure 43. The blue and dark grey structure represents the fixed piece, the one that has to be tied to the lower grip of the tensile machine, while the green and light grey structure is the mobile one, which is screwed to the first piece once the retina sample has been transferred on the clamp instrument. The designed test chamber will be transparent, it has been designed in this way to better distinguish the individual components. Appendix A instead shows the 3D drawings from every perspective as well as the technical bidimensional drawing.

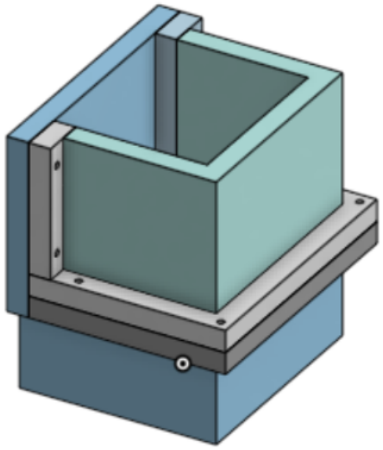

Figure 43 Designed test chamber

3.4 Mechanical parameters calculation

At the end of the tests, stress and strain parameters of the tissue were calculated through Excel. The stress (kPa) is defined as the ratio of the applied force (N) to the original cross section area (mm^2), while the strain (mm/mm), is defined as the change of length divided by L_0. The original cross section area was calculated as the multiplication of the initial thickness of the sample by the initial width. Then, stress-strain graph was plotted for each sample.

Then the Young's modulus (E) was extracted from the stress-strain plot as the angular coefficient of the linear portion of the curve before the change of the slope. We also considered in our analysis the yield stress (σ_y), defined as the point of change of slope in the

first linear elastic region of the stress-strain curve, the failure stress, which was set to the stress value after which there was a clear descent of the curve, and the failure strain, defined as the strain value corresponding to the failure stress.

3.5 Statistical analysis

All data are reported as mean and standard deviation calculated using Excel.

Furthermore, between the two families of samples tested with the TC3F tensile machine, retina specimen with and without optic nerve, a t-student test was carried out in order to determine whether using the optic nerve as a grab could affect the calculation of the Young's modulus.

3.6 Digital Image Correlation (DIC)

Following some differences highlighted between the deformations calculated at the end of tensile tests performed with TC3F and EnduraTEC machines, we decided to carry out an additional analysis.
The *Digital Image Correlation* (DIC) is a non-invasive optical measuring instrument that allows the measurement of displacements and deformations on surfaces of objects subjected to solicitation. It is based on monitoring unique details visible on the surface through the numerical elaboration of digital images: by analyzing the gray values on the frames, the deformations and three-dimensional displacements are quantified.

DIC applications are wide in so many fields including the investigation of mechanical properties of biological tissues. To do this it is necessary to create a high contrast pattern on the surface of the biological sample. The preparation of the surface must be carried out quickly and without dehydration of the tissue to avoid alterations in its mechanical properties.

In this paragraph the DIC working principle, the algorithm used and the techniques most used for the generation of patterns on biological tissues will be illustrated. Finally, the application of this measurement's technique on the retina samples will be described.

The working principle of DIC, schematized in Figure 44, is based on the comparison in terms of color in grayscale of specific areas of the sample before and after the deformation.

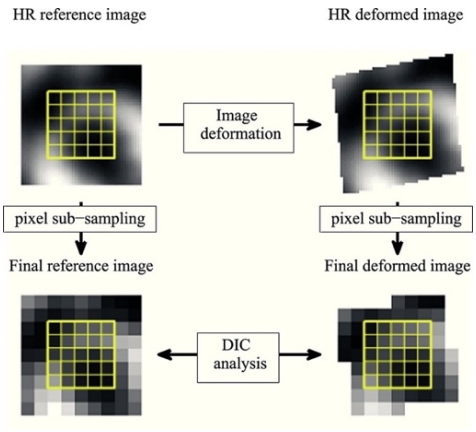

Figure 44 Scheme of the working principle of DIC analysis

The procedure is based on recording through a camera the sample while subjected to mechanical stress: in our case tensile force. Subsequently, digital images are extracted and processed using a correlation algorithm to calculate the sample deformation field (Figure 45).

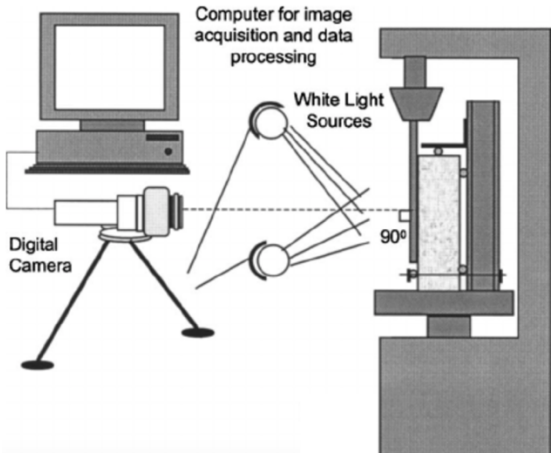

Figure 45 DIC procedure: acquisition of digital images and data processing

The goal is to find the correspondence between the same points in images recorded before and after the deformation of the specimen. The before and after images are called “reference image” and “deformed image” respectively. The analysis is performed within a specific area chosen in the reference image called *Region of Interest* (ROI). Subsequently, the algorithm searches within deformed images of the sample for those areas that have the greatest similarity with the ROI of the original image. DIC does this by taking small subsections of the reference image, called *subsets*, and determining their respective locations in the current configuration (Figure 46). Finally, by means of this correlation, strains and the deformation field are calculated.

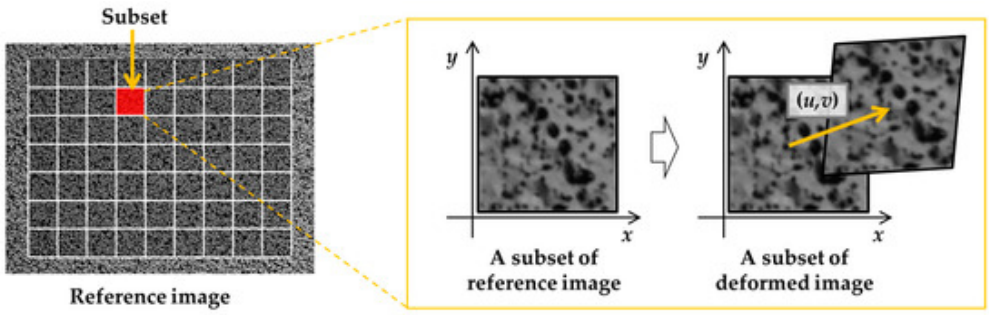

Figure 46 Scheme of the reference subset and the deformed subset

Since DIC analysis is based on monitoring unique details visible on the sample surface, a high contrast pattern must be present on the surface. When analyzing biological tissues, patterns should neither cause or require sample dehydration, nor alter the mechanical response, but they should adhere to the tissue surface and withstand large deformations [17]. Below, some popular techniques for the generation of patterns on biological tissue are reported with respective advantages and disadvantages.

A first technique involves the *use of powders*, such as toner. In this case the advantage lies in the fact that the use of spherical particles of powders with controllable size should guarantee the desired pattern size. However, the adhesion of the powders to the surface of the sample is not reliable over time and its detachment can affect the measurements made by DIC.

Another method for the generation of patterns on biological tissues consists in the use of *powder ink combined with gelatinous substances*. In this case there is a better adhesion of

the powders to the tissue compared to the previously described technique thanks to the gelatin. However, the protocol requires the application of a thin and homogeneous film on the surface of the sample and this is particularly difficult on soft and irregular shaped samples.
The last technique that is described concerns the *use of paints or dyes* which can be deposited by means of an airbrush on the surface of the biological sample. This is the case in which the adhesion of the material on the surface is maximum. The problem, not negligible, lies in the fact that the use of these substances could alter the mechanical response of the fabric.

Among the techniques described for the creation of high contrast patterns on the surface of biological tissues, the choice for retina samples fell on the use of powders, in particular toner.

The protocol devised is based on the use of a toothbrush to create the pattern, as shown in Figure 47. Once the sample has been transferred between the clamps, the brush is dirtied with the toner and its bristles are moved with a finger. In this way, the toner powder is deposited spontaneously on the surface of the sample, creating a dotted pattern which should be as dense as possible. Subsequently the tensile test is started and is recorded for its entire duration through a high definition camera (CANON EOS 6D, lens CANON MP-E 65 mm f/2.8 1-5x) installed on a tripod. The frames which will then be used for DIC will be then extracted from the video with a Matlab code.

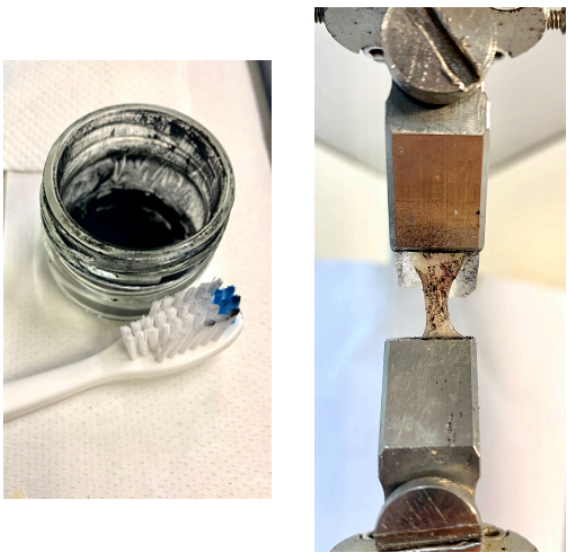

Figure 47 Creation of the pattern on the surface of retina sample through the use of toner and toothbrush

Regarding this thesis project, 100 frames were extracted from a time interval considered significant for the purposes of the analysis. The obtained images were then be input to Ncorr, an open source 2D digital image correlation Matlab program, for the calculation of the strains.

First, the reference image was set. The *File > Load Reference Image* command opens a window of the type shown in Figure 48, from which it is possible to load the reference image, the first image you take of the sample before any deformation occurs. Subsequently, the other images that have previously described as “deformed images” were loaded using the *File > Load Current Images* command (Figure 49).

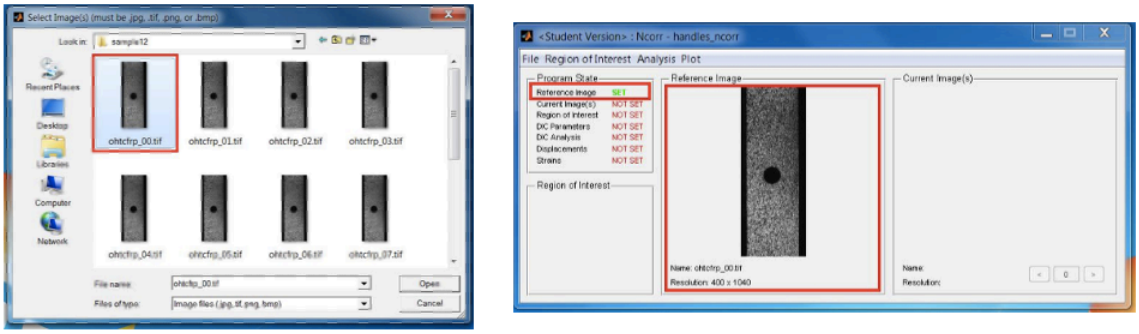

Figure 48 Setting of the reference image

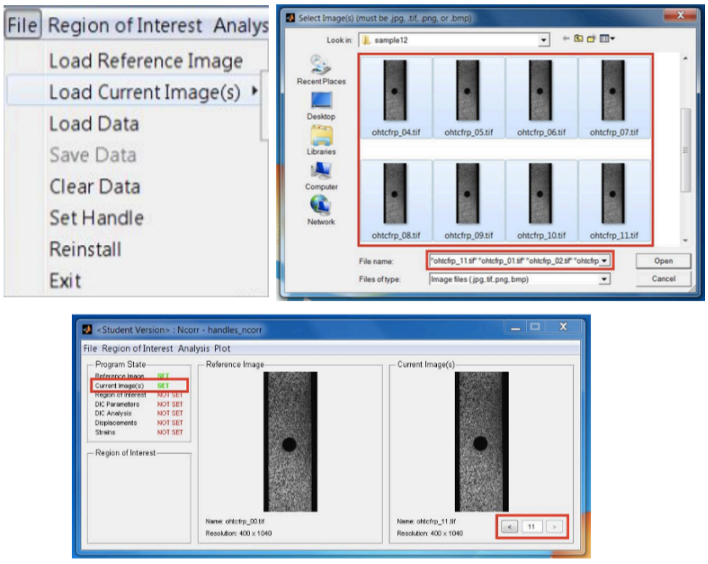

Figure 49 Setting current images

The next step concerns the choice of the region of interest (ROI), or the region within which the program calculates the field of deformation. Generally, the area of interest is chosen where the pattern is denser and uniform. To do this we used the commands *Region of Interest > Set Reference ROI > Draw ROI.* This allows us to draw the ROI directly to our liking on the reference image (Figure 50).

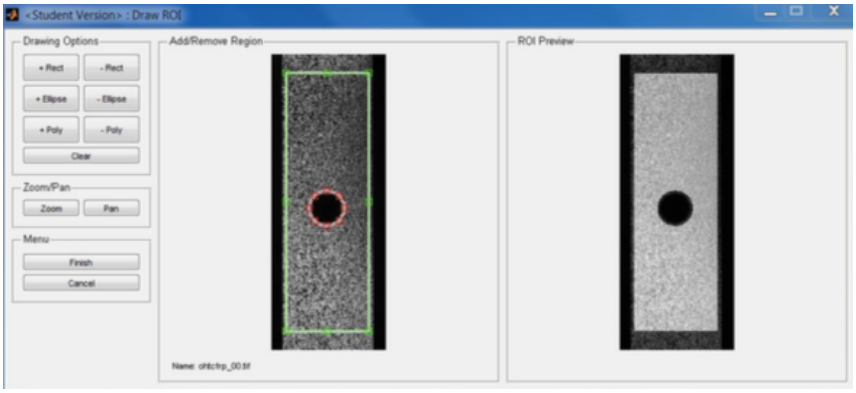

Figure 50 Setting of the ROI through the Draw ROI command

Once the ROI has been defined, the parameters for the DIC analysis are set. Using the *Analysis > Set DIC Parameters* command, the window shown in Figure 51 opens. For simplicity, only the main parameters that belong to the *Subset Options*, circled in red, and *Iterative Solver Options*, circle in blue, categories will be described. Regarding the Subset Options these are the main components of the DIC analysis: The *Subset Radius* defines the size of the subset, how large it should be, while the *Subset Spacing* dictates the distance between subsets. In our analysis they were set at 30 and 3 respectively. Overall, the main idea is to select the smallest subset possible which does not result in noisy displacement data. As regards the Iterative Solver Options, we refer to the *Relative Error*, set by default at 1e-006, and to the *Number of Iterations*, which in our case is fixed at 100.

Figure 51 Ncorr main parameters for DIC analysis

Once the parameters have been properly set, the DIC analysis can be started. All Matlab codes for the calculation of the parameters and the output graphs are shown in Appendix B, together with the explanation of the correlation algorithm and the code for the extraction of the input data frames. It is necessary to say that this analysis calculates the strains both in *Green-Lagrangian* and *Eulerian-Almansi* configurations. The physical reality is the same but the Lagrangian strain is defined as the change in length divided by the original length, while Eulerian strain is defined as the change in length divided by the instantaneous length. The Lagrangian and Eulerian strain can be respectively calculated as:

$$\varepsilon_L = \frac{\Sigma \Delta L}{L_0} \qquad and \qquad \varepsilon_E = \sum \frac{\Delta L}{L} \qquad [mm/mm]$$

For convenience, the code also calculates the logarithmic strain so that the result is independent of the two types of configurations. The logarithmic strain is calculated as:

$$\varepsilon_{log} = \log(\sqrt{\lambda}) \quad [mm/mm]$$

Where λ is the *stretch ratio* defined by the relationships:

$$\lambda = \frac{L}{L_0} \ [mm/mm]$$

$$and$$

$$\varepsilon = \lambda - 1$$

Regarding the Langrangian configuration the stretch ratio can be calculated as:

$$\lambda_{Lag} = 2 \times \varepsilon_{Lag} + 1$$

While in the Eulerian configuration as:

$$\lambda_{Eul} = \frac{1}{(1 - 2 \times \varepsilon_{Eul})}$$

As regards this thesis project, being the results preliminary, only two types of obtained plot will be described in the results: the color map of the gradient of deformation in the Eulerian configuration and the curve of the logarithmic strain in the direction of the applied force (y axis) for each frame (x axis).

Chapter 4: Results

In this chapter the results deriving from each analysis performed during this thesis project and useful for the biomechanical characterization of the porcine retina are reported. In particular, we will pass from the estimation of the thickness of retinal samples obtained by optical coherence tomography, to the values of the biomechanical parameters calculated after the various tensile tests performed on retinal specimens. Finally, the preliminary results regarding the DIC analysis for the estimation of the deformation fields will be reported.

4.1 Retinal thickness measurements by OCT

As previously described in the paragraph 3.2, optical coherence tomography was performed on three pig eyes with the aim of estimating the retinal thickness, essential for the calculation of the biomechanical parameters. Subsequently, an image processing was performed: for each of the three obtained images, one of which is shown in Figure 52, the thickness in three different areas of the retina was estimated. In this way: for each sample we obtained four retinal thickness measurements, the first deriving from the OCT and the other three from the analysis performed with ImageJ. This analysis was carried out in such a way as to obtain a final mean value that could be used for all retinal samples without optic nerve.

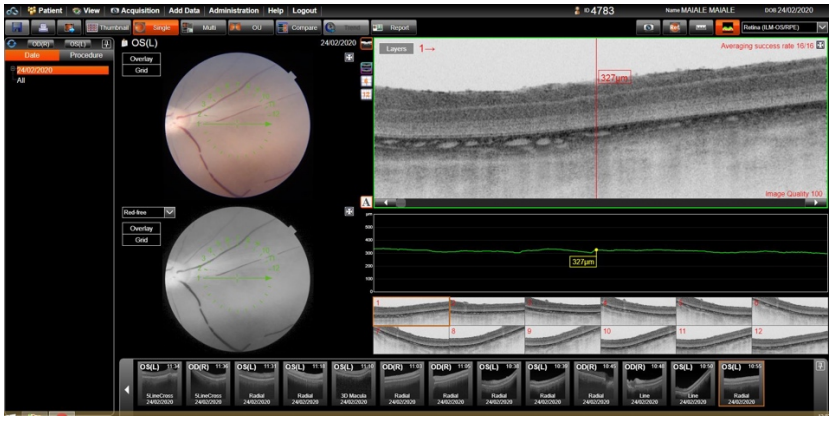

Figure 52 Image obtained from OCT analysis

Table 6 shows the retinal thickness measurements for each of the three samples. The first column corresponds to the measurement returned by the OCT, followed by the values obtained through ImageJ and, finally in the last column, the average of the four values. Instead, Table 7 reports the final average value with its standard deviation, used for the calculation of the biomechanical parameters of the retinal samples without optic nerve, and obtained from the average of the three average values previously calculated.
It is believed that this analysis was a valid and effective idea to obtain an average value that could be used for all the analyzed samples without optic nerve. In fact, the average value obtained following the image processing carried out on the three tomographic images (351.75 µm ± 38.45) is consistent with the range of values found in literature according to which the retinal thickness of pig's eyes ranges from 300 to 400 µm [19].

Sample	OCT measure [µm]	ImageJ measure 1 [µm]	ImageJ measure 2 [µm]	ImageJ measure 3 [µm]	Average measure [µm]
1	327	303	319	331	320
2	353	345	353	312	340.75
3	408	367	422	381	394.5

Table 6 Thickness measurements

Final Average Thickness Value [µm]	Standard Deviation
351.75	38.45

Table 7 Final average value of retinal thickness and standard deviation

4.2 Tensile tests performed with TC3F machine

This paragraph reports the results of the mechanical tensile tests performed with the force measurements tensile machine (EBERS, TC3F). In particular, the results are related to the obtaining of the stress-strain curve, plotted after the calculation of stress and strains starting from the parameters returned by the software, and the biomechanical parameters, for both samples with optic nerve and without it. Finally, the results related to the t-test carried out

with the aim of determining whether the use of the optic nerve as a grip could influence the calculation, in particular, of the Young's modulus will be reported.

Below are reported the results of the tensile tests carried on 9 samples with optic nerve. Figure 53 shows one of the stress-strain curves obtained (sample 2). The curve is characterized by an initial short linear region followed by a larger plastic zone. The continuous change in slope of the curve could be due to the fact that the sample attached to the optic nerve is a packing of portions of the retinal tissue presumably of different lengths and therefor some parts could break before others. The orange line represents the linear tract considered for the calculation of the Young's modulus, which corresponds to the angular coefficient.

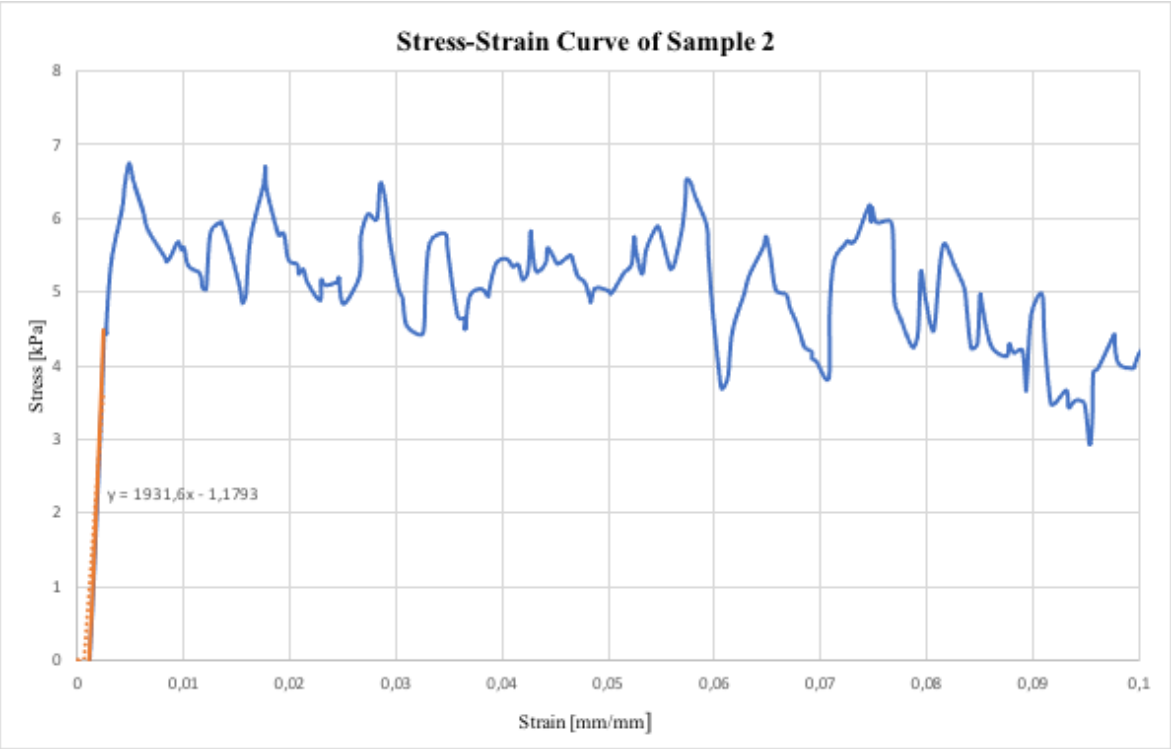

Figure 53 Stress-strain curve of the sample 2 with optic nerve. On x-axis the strains are reported in [mm/mm] while on y-axis stresses are reported in [kPa]

The fundamental biomechanical parameters were then extracted from the curve, reported for each sample in Table 8. Table 9 instead contains the average values of the calculated parameters and the respective standard deviations. In particular, the following values were obtained: average Young's modulus equal to 1835 ± 1.35 kPa, average yield stress of 3.03 ± 2.23 kPa, average value of failure stress equal to 7.46 ± 5.8 kPa and average failure strain of 0.089 ± 0.1 mm/mm.

Sample	Young's Modulus [kPa]	Yield Stress [kPa]	Failure Stress [kPa]	Failure Strain [mm/mm]
1	5000	6.56	8.48	0.016
2	1932	6.48	6.28	0.057
3	2213	3.58	19.25	0.3
4	1778	3.24	13.34	0.26
5	2189	1.28	3.32	0.056
6	560	0.93	2.07	0.024
7	540	0.4	1.63	0.021
8	1024	2.25	4.56	0.049
9	1276	2.54	8.18	0.015

Table 8 Values of the calculated biomechanical parameters of each sample with optic nerve

Average Young's Modulus [kPa] ± SD	1835 ± 1.35
Average Yield Stress [kPa] ± SD	3.03 ± 2.23
Average Failure Stress [kPa] ± SD	7.46 ± 5.8
Average Failure Strain [mm/mm] ± SD	0.089 ± 0.1

Table 9 Average values of the main parameters and standard deviation with optic nerve

As for the case of the samples with optic nerve, the tensile tests were also carried out on 9 specimens without optic nerve, folded in 2 or 4 layers and hydrated thanks to the presence of PBS. The procedure and the calculated parameters are the same. Figure 54 shows a curve obtained from one of the tests performed on this type of sample (sample 3). As in the previous case, the curve is characterized by a short linear region, corresponding to the elastic

zone, followed by a wider plastic region characterized in turn by continuous changes in slope probably due to micro-fractures.

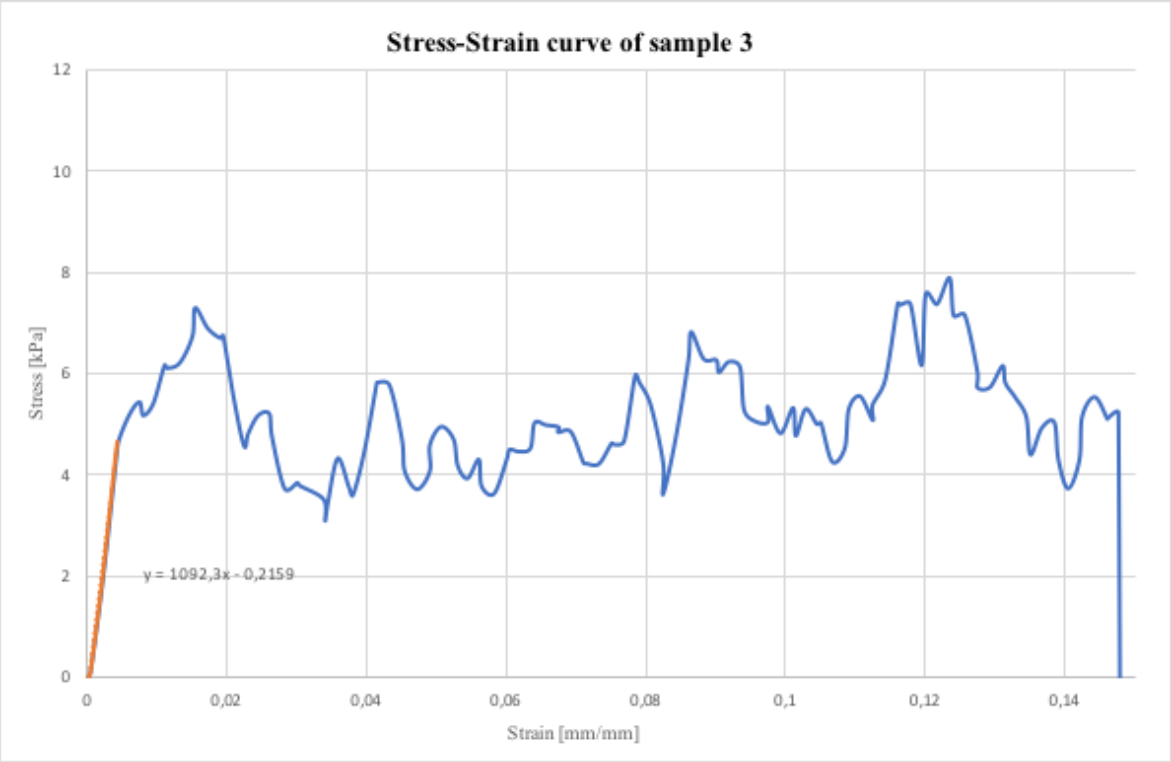

Figure 54 Stress-strain curve of the sample 3 without optic nerve. On x-axis the strains are reported in [mm/mm] while on y-axis stresses are reported in [kPa]

Table 10, as in the previous case, reports the biomechanical parameters extracted from the stress-strain curve, while Table 11 shows the average values of the parameters and the respective standard deviations. In this case we obtained an average Young's modulus equal to 3470 ± 3.09 kPa, a mean value of yield stress of 9.15 ± 6.09 kPa, an average failure stress of 9.76 ± 6.1 kPa and a mean failure strain of 0.113 ± 0.2 mm/mm.

Sample	Young's Modulus [kPa]	Yield Stress [kPa]	Failure Stress [kPa]	Failure Strain [mm/mm]
1	7500	18.3	20.7	0.7
2	816	6.1	7.7	0.019
3	1092	7.3	5.23	0.147
4	434	4.4	8.94	0.038
5	3700	11.3	8.4	0.008
6	1700	5.3	6.6	0.033
7	7300	11	10.7	0.023
8	1285	0.51	1.5	0.015
9	7411	18.1	18.1	0.035

Table 10 Values of the calculated biomechanical parameters of each sample without optic nerve

Average Young's Modulus [kPa] ± SD	3470 ± 3.09
Average Yield Stress [kPa] ± SD	9.15 ± 6.09
Average Failure Stress [kPa] ± SD	9.76 ± 6.1
Average Failure Strain [mm/mm] ± SD	0.113 ± 0.2

Table 11 Average values of the main parameters and standard deviation without optic nerve

As regards the experimental tests performed with the force measurement bioreactor (EBERS, TC3F), the trends of the obtained stress-strain curves are similar to those of the curves present in the pre-existing works, both in the case of samples with and without optic nerve. However, in both cases, the calculated biomechanical parameters turned out to be notably different from those of the works in the literature. In particular, the biggest problem concerned the strain values. If, for example, in the values present in literature the yielding occurred in the vicinity of strains between 2% and 10%, the values in the curves we obtained do not even reach the 1% in most cases. This clearly also influenced the values of the Young's modulus, a parameter on which in particular we have placed our attention, which in our case is 1-2 orders of magnitude greater. The answer we gave ourselves to this difference was that probably the used tensile machine does not acquire a sufficient number of points to calculate the biomechanical parameters of the tissue in question in a satisfactory

way. This was one of the reasons that led us to consider the option of carrying out the tensile tests with a second machine.

Finally, a t-test was performed to determine whether the use of the optic nerve as a grip could affect the calculation of the biomechanical parameters and, in particular, the Young's modulus. By comparing the Young's modulus values of the two sample families, there is no statistical significance ($P > 0.05$) that attests that using one protocol yields different results than the other.

4.3 Tensile tests performed with EnduraTEC machine

After having calculated the biomechanical parameters following the tests performed with TC3F and having found differences in particular between the obtained strain values and those present in the literature, we thought it might be interesting to compare the same protocol performed on two different machines. For this reason, the tests on samples without optic nerve were also carried out with the BOSE EnduraTEC tensile test machine. In particular, following the previously performed t-test, we decided to focus only on samples without optic nerve as they allowed to have a thickness value as precise as possible, despite being more difficult to fit between the grips.
The test parameters (i.e., test velocity 0.1 mm/s) are the same as in the previous tests, as well as the outputs. Also in this case, in fact, at the end of each test, stresses and strains were calculated, the curve plotted, and the fundamental biomechanical parameters extracted from it. Below, numerical results concerning these tests are reported.

Tests were performed on 16 samples without optic nerve and Figure 55 shows one of the stress-strain curves obtained. The trend or the curve is consistent with both those of the test carried out with TC3F and with those present in previous works, being characterized by a short elastic phase followed by a larger plastic region. Differently from the curves described in the previous paragraph (4.2), relating to the tests carried out with TC3F, the curve in Figure 55 appears to have a more regular and less fluctuating trend. This could be due to a better sample fitting, easier on the EnduraTEC, or to the absence of PBS. In fact, the presence of the latter is advantageous as it allows to carry out tests in physiological conditions, but it could also cause micro-fractures in the retinal sample during the addition in the test chamber.

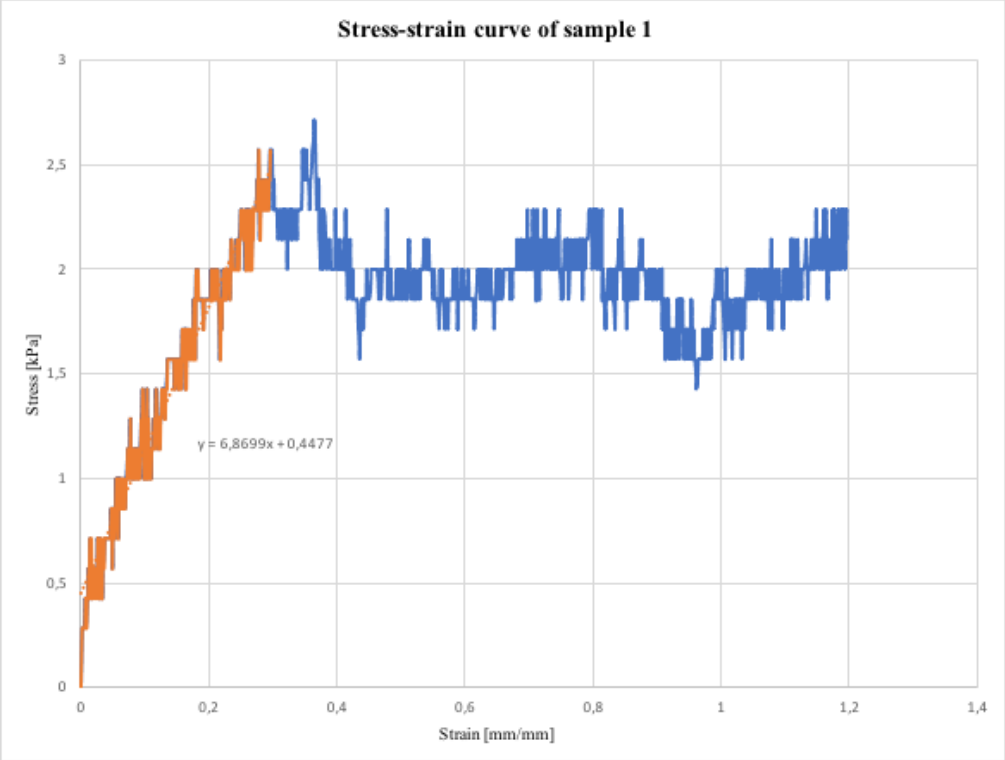

Figure 55 Stress-strain curve of the sample 1 without optic nerve. On x-axis the strains are reported in [mm/mm] while on y-axis stresses are reported in [kPa]

Table 12 reports all the biomechanical parameter calculated for each sample while Table 13 shows the average values and standard deviations. In particular we obtained an average Young's modulus equal to 13.4 ± 0.0067 kPa, a mean value of yield stress of 1.33 ± 0.75 kPa, an average failure stress of 2.21 ± 0.8 kPa and a mean value of failure strain equal to 0.66 ± 0.3 mm/mm.

Sample	Young's Modulus [kPa]	Yield Stress [kPa]	Failure Stress [kPa]	Failure Strain [mm/mm]
1	7	2.57	2.28	0.84
2	18	0.85	1.85	0.41
3	16	0.8	1.49	0.28
4	12	0.57	0.86	0.23
5	7.5	0.66	1.05	0.74
6	9	1.05	2.66	0.97
7	19	0.71	2.28	0.97
8	4	1.4	3.14	0.71
9	14	1.33	2.67	0.83
10	26	0.85	1.57	0.62
11	10	0.91	2.05	0.77
12	15	2.74	3.65	0.89
13	10	1.43	2.71	0.83
14	27	2.86	3.71	0.36
15	14	1.37	1.82	0.78
16	6	1.14	1.52	0.36

Table 12 Values of the calculated biomechanical parameters of each sample without optic nerve

Average Young's Modulus [kPa] ± SD	13.4 ± 0.0067
Average Yield Stress [kPa] ± SD	1.33 ± 0.75
Average Failure Stress [kPa] ± SD	2.21 ± 0.8
Average Failure Strain [mm/mm] ± SD	0.66 ± 0.3

Table 13 Average values of the main parameters and standard deviation without optic nerve

4.4 Preliminary results of DIC analysis

As described in paragraph 3.6, in the final phase of this thesis project we wanted to experiment the DIC analysis on retinal samples in order to estimate the strain fields during the tensile tests. In particular, this idea was driven by the fact by the fact that the deformation values of the two used protocol were very different from each other. The results are only preliminary. In fact, the analysis has been applied to only a couple of samples whereas it requires a lot of specimens to set the parameters in the most appropriate way possible. A first goal was certainly to be able to perform the analysis with the created pattern, although they should be denser and more uniform to consider a ROI as broad as possible.

The two outputs we focused on are shown in Figure 56 and Figure 57. In the first case the colorimetric map of the deformations according to the Eulerian configuration in the direction of the force applied to the sample is shown. The map shows a uniform deformation gradient with values coherent with those obtained from the performed experimental tests carried out with EnduraTEC machine.

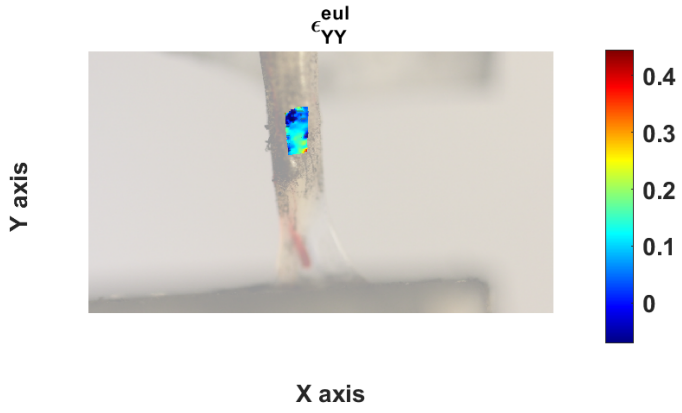

Figure 56 Colorimetric map with respect to the Eulerian component ε_{yy}

Finally, in Figure 57, the logarithmic deformations calculated for each frame used for the analysis is reported. In this particular case, the initial decreasing trend of the curve could be due to an initial compression phenomenon due to the relative flow between the layers in which the retina is folded during the tensile test. The numerical values are consistent with those previously calculated.

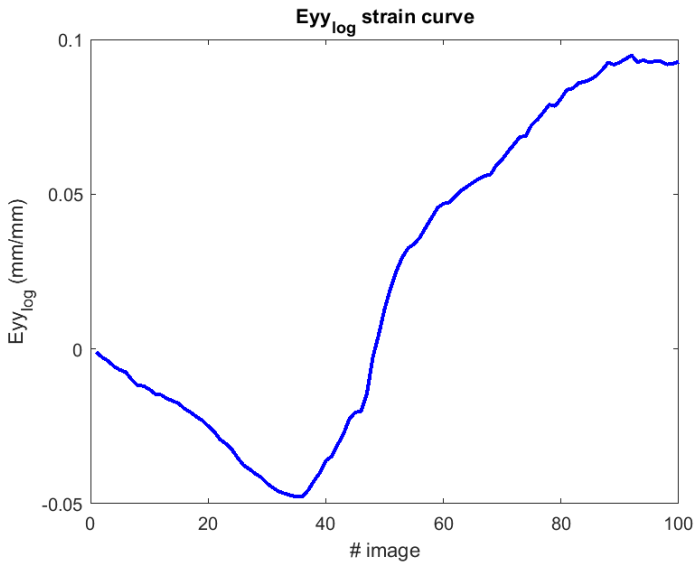

Figure 57 Curve representing the logarithmic deformations calculated for each frame

Chapter 5: Conclusions and future developments

The main aim of this project was to perform a biomechanical characterization of the porcine retina starting from considerations made on retinal detachment, a pathological condition in which the mechanics of the tissue is directly involved. This work is essential for the implementation of pre-existing or new surgical techniques or the generation of computational models that can simulate the disease and its treatment

To do this, tensile tests were carried out on retina samples at the end of which some fundamental biomechanical parameters, i.e. Young's modulus, yield stress, failure stress and failure strain, were calculated. In our case, a travel ramp has been applied to the upper grip with a speed equal to 0.1 mm/s.

At first the tests were carried out with the TC3F test machine on retinal samples attached to the optic nerve, used as a grip, and without optic nerve but folded in 2 or 4 layers. In this second case the tests were also performed in presence of PBS. In the case of sample with optic nerve there was less difficulty in grabbing the sample but less precision in the evaluation of the thickness, essential for the calculation of biomechanical parameters. On the contrary in specimens without optic nerve there was a more precise estimate of the thickness, performed through Optical Coherence Tomography, but less comfort in the grasping of the tissue.

At the end of the tests, starting from the parameters returned by the software, stresses and strains were calculated, the stress-strain curves plotted, and, from them, the biomechanical parameters extracted. In this case the numerical value, in particular those relating to deformations, and consequently also those of the Young's modulus, were found to be considerably different from those present in literature. This is probably due to the fact that the used tensile machine does not acquire a sufficient number of points to calculate the biomechanical parameters of the retina in a satisfactory way. To verify this hypothesis, in the future, it would be interesting to perform the same test with the same input parameters on a material with a known Young's modulus. In any case, despite the inaccuracy of the calculated parameters, these first experimental tests allowed us to determine that using the optic nerve as a grip does not affect the calculation of the biomechanical parameters

compared to the test on samples without optic nerve, being the values of Young's modulus comparable between the two populations.

Since the calculated parameters were evidently different from those found in literature, further tests were carried out on the samples without optic nerve, always following the same protocol, with EnduraTEC test machine. In this case, the values of the calculated biomechanical parameters turn out to be more similar to the values present in previous works. This support the hypothesis on the experimental results previously analyzed. However, in this case, it was not possible to perform wet tests due to the fact that the preexisting test chamber has proven to be unsuitable for retinal specimens. For this reason, as for the future development, it would certainly be interesting to create the test chamber designed and described in paragraph 3.3.2.1 and carry out tensile tests in the presence of PBS with the aim of mimicking the physiological conditions of the tissue.

Finally, to confirm the obtained results, a DIC analysis was performed on a couple of retina samples. Although the results are only preliminary, the colorimetric map of the deformations and the curve of the logarithmic deformations calculated for each frame, return values consistent with those result from the tensile tests performed with EnduraTEC machine.
In the future, it would be interesting to try to get a denser and more uniform pattern than the one obtained with the toner in order to be able to consider a more extensive ROI, which in our case was not possible. The method of creating the pattern could be changed, as the deposition of toner on the already mounted retina sample has proved to be quite difficult. For example, we could thick of spraying paint drops with the use of an airbrush. Moreover, it will be necessary to carry out the analysis on a larger number of samples, in order to verify the authenticity of the results. Finally, the Young's modulus could be calculated also using the strain values obtained from the DIC analysis and the stresses obtained starting from the force values returned by the tensile machine software. To do this, it would be necessary to perform a synchronization between the forces recorded by the tensile machine used for the calculation of the stress values and the frames extracted from the video and used for DIC analysis which returns the strain values.

In conclusion, the biomechanical parameters obtained from the analyzes performed are in line with those found in literature that define the retina as a fragile tissue with a biomechanical behavior characterized by a short elastic phase followed by a large plastic phase before the rupture.

Appendix A

Test chamber design for wet testing

Below are the 3D drawings and technical tables related to the test chamber designed for the BOSE EnduraTEC tensile machine which could be built with the aim of performing tests in physiological conditions. The chamber test would be made of transparent Plexiglas. In the drawings the different components are colored to allow distinction.

3D drawings

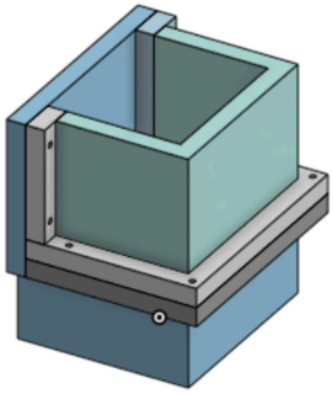

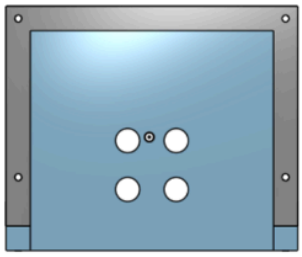

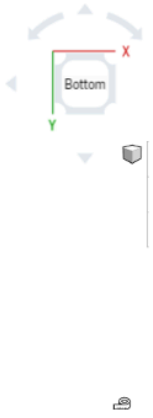

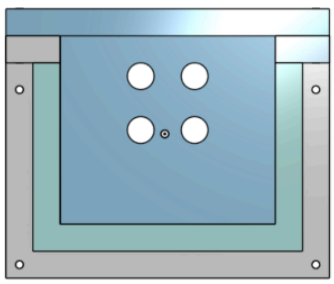

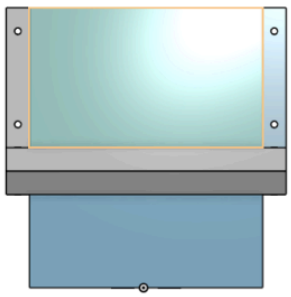

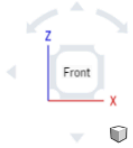

Technical tables

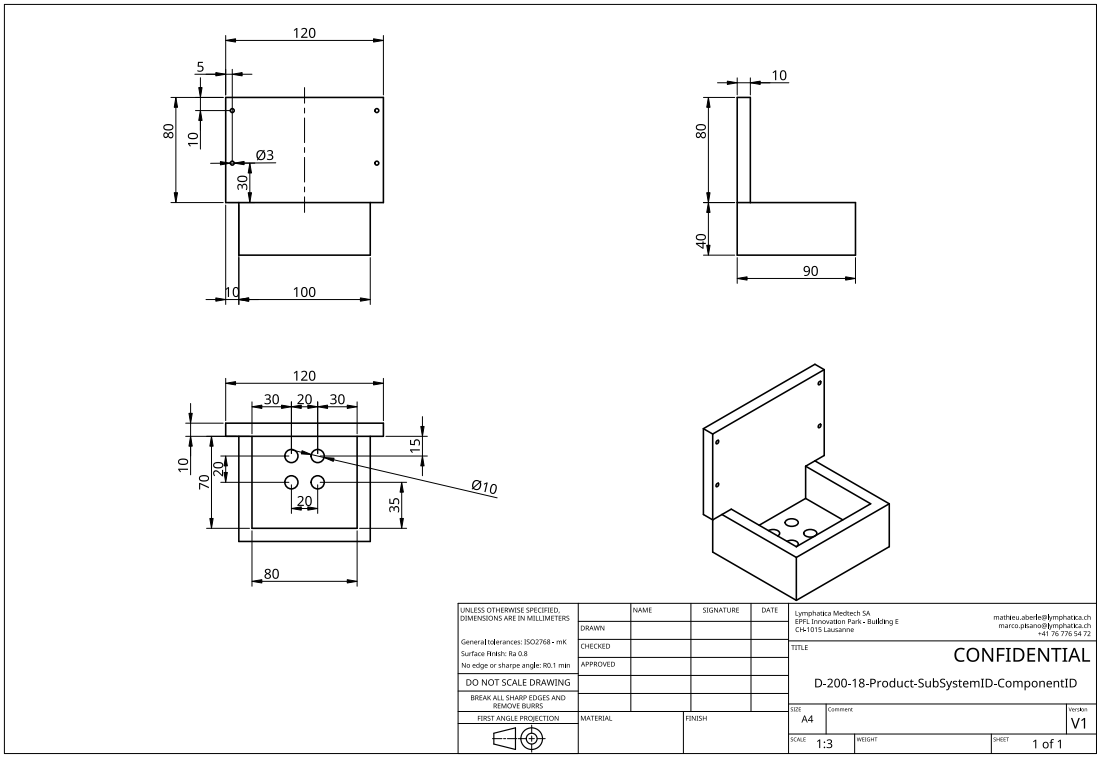

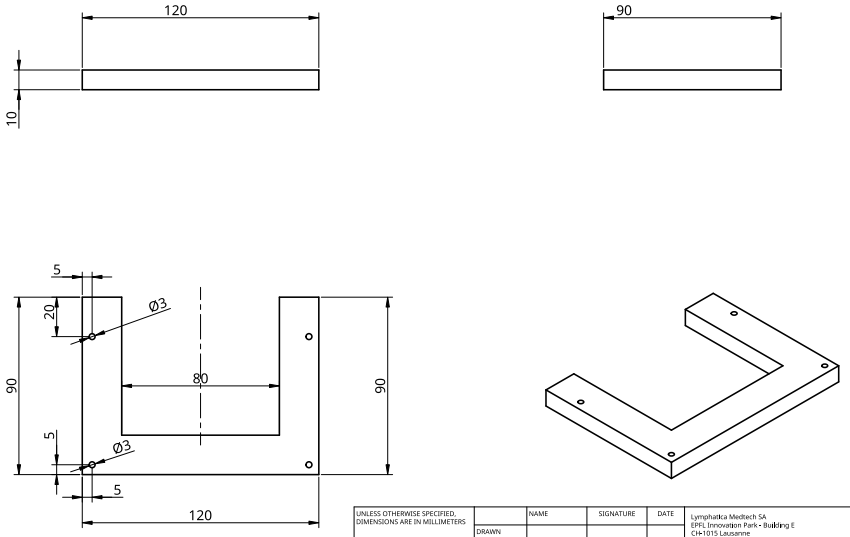

UNLESS OTHERWISE SPECIFIED, DIMENSIONS ARE IN MILLIMETERS		NAME	SIGNATURE	DATE
General tolerances: ISO2768 - mK	DRAWN			
Surface Finish: Ra 0.8	CHECKED			
No edge or sharpe angle: R0.1 min	APPROVED			
DO NOT SCALE DRAWING				
BREAK ALL SHARP EDGES AND REMOVE BURRS				
FIRST ANGLE PROJECTION	MATERIAL		FINISH	

Lymphatica Medtech SA
EPFL Innovation Park - Building E
CH-1015 Lausanne

mathieu.aberle@lymphatica.ch
marco.pisano@lymphatica.ch
+41 76 776 54 72

TITLE

CONFIDENTIAL

D-200-18-Product-SubSystemID-ComponentID

SIZE	Comment	Version
A4		V1

SCALE	WEIGHT	SHEET
1:2		1 of 1

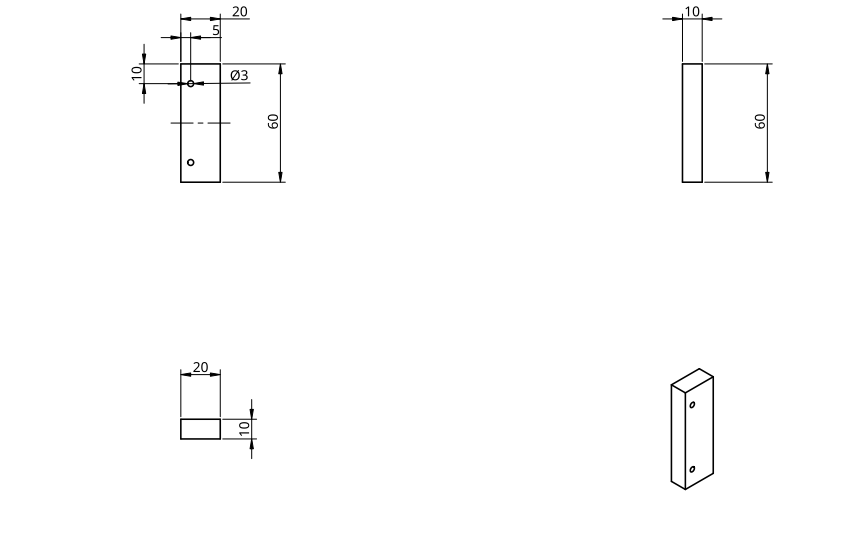

UNLESS OTHERWISE SPECIFIED, DIMENSIONS ARE IN MILLIMETERS		NAME	SIGNATURE	DATE
General tolerances: ISO2768 - mK	DRAWN			
Surface Finish: Ra 0.8	CHECKED			
No edge or sharpe angle: R0.1 min	APPROVED			
DO NOT SCALE DRAWING				
BREAK ALL SHARP EDGES AND REMOVE BURRS				
FIRST ANGLE PROJECTION	MATERIAL		FINISH	

Lymphatica Medtech SA
EPFL Innovation Park - Building E
CH-1015 Lausanne

mathieu.aberle@lymphatica.ch
marco.pisano@lymphatica.ch
+41 76 776 54 72

TITLE

CONFIDENTIAL

D-200-18-Product-SubSystemID-ComponentID

SIZE	Comment	Version
A4		V1

SCALE	WEIGHT	SHEET
1:2		1 of 1

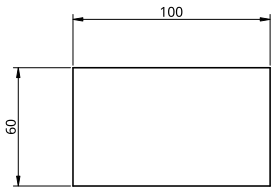

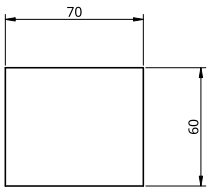

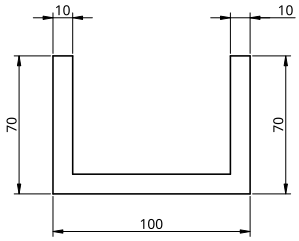

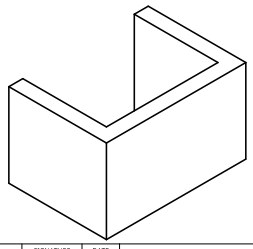

UNLESS OTHERWISE SPECIFIED, DIMENSIONS ARE IN MILLIMETERS		NAME	SIGNATURE	DATE
General tolerances: ISO2768 - mK	DRAWN			
Surface Finish: Ra 0.8	CHECKED			
No edge or sharpe angle: R0.1 min	APPROVED			
DO NOT SCALE DRAWING				
BREAK ALL SHARP EDGES AND REMOVE BURRS				
FIRST ANGLE PROJECTION	MATERIAL		FINISH	

Lymphatica Medtech SA
EPFL Innovation Park - Building E
CH-1015 Lausanne

mathieu.aberle@lymphatica.ch
marco.peano@lymphatica.ch
+41 76 776 54 72

TITLE

CONFIDENTIAL

D-200-18-Product-SubSystemID-ComponentID

SIZE	Comment	Version
A4		V1

SCALE	WEIGHT	SHEET
1:2		1 of 1

Appendix B

Below, the algorithm on which DIC analysis is based and the Matlab codes used to extract the frames used for the analysis and to calculate the outputs will be shown.

DIC analysis algorithm

In order to determine the similarity between the reference subset and the deformed subset, different correlation coefficient can be used among which the most common are:

- The sum of the absolute value of the differences (SAD);
- The sum of the squared differences (SSD);
- The cross-correlation (CC).

The cross-correlation between reference and deformed subsets of (2M + 1) X (2M + 1) pixels is based on the Zero-mean Normalized Sum of Squared Differences (ZNSSD) correlation coefficient:

$$C_{ZNSSD} = \sum_{i}^{M}\sum_{i}^{M}\left[\frac{f(x,y)-f_m}{\sqrt{\sum_{i=M}^{M}\sum_{i=-M}^{M}\left(f(x,y)-f_m\right)^2}} - \frac{g(x',y')-g_m}{\sqrt{\sum_{i=M}^{M}\sum_{i=-M}^{M}\left(g(x',y')-g_m\right)^2}}\right]$$

$$f_m = \frac{1}{2M+1}\sum_{i=M}^{M}\sum_{i=-M}^{M} f(x,y) \quad , \quad g_m = \frac{1}{2M+1}\sum_{i=M}^{M}\sum_{i=-M}^{M} g(x',y')$$

Where f (x; y) is the gray intensity at coordinates (x; y) in the undeformed image, g (x'; y') is the gray intensity at coordinates (x'; y') in the deformed image and are, respectively, the mean grey values in the reference and deformed subsets.

Matlab code for extracting frames

```
time_start=7; % s
% time_end=video_time_tot;
time_end=39;  % s

n=100+1;

v = VideoReader('MVI_2034_coloratapost.mp4');
h=v.Height;
w=v.Width;
video=zeros(h,w,3);
time=linspace(time_start,time_end,n);

for i=1:n
    v = VideoReader('MVI_2034_coloratapost.mp4','CurrentTime',time(i));
    image = readFrame(v);
    name=sprintf('immagine_%0.f.tif',i-1);
    imwrite(image,name);
end

frame_rate=v.FrameRate;
video_time_tot=v.Duration;
numFrames = ceil(frame_rate*video_time_tot);
frame_start=1+frame_rate*time_start;
frame_start=round(frame_start);
frame_end=frame_rate*time_end;
frame_end=round(frame_end);

index=linspace(frame_start,frame_end,n);
index=round(index);
```

Matlab code for the calculation of DIC outputs

```
% Green-Lagrange strain (reference ROI)
% Almansi-Eulero strain (current ROI)
% Config = 'Lagrange';
Config = 'Eulero';

% Inserire l'indirizzo della cartella dove c'è il programma Ncorr.m
cd('C:\Users\mstefanati\Desktop\2020\DIC retina\ncorr_2D_matlab-master')
handles_ncorr = ncorr;
% Inserire l'indirizzo della cartella dove ci sono le immagini da
% analizzare
cd('C:\Users\mstefanati\Desktop\2020\DIC retina\Test_color_pre\images_tot')

load 'results_R30_S3_SR3_noHigh.mat'

k=length(data_dic_save.strains);
time=k;
spac=data_dic_save.dispinfo.spacing;

if strcmp(Config,'Lagrange')
    img = imread('immagine_0.tif');

    [m,n]=size(reference_save.roi.mask);
    ROI=zeros(m,n);
    % ROI=reference_save.roi.mask;
    ROI(reference_save.roi.mask)=1;
end
if strcmp(Config,'Eulero')
    img = imread('immagine_100.tif');

    [m,n]=size(current_save(end).roi.mask);
    ROI=zeros(m,n);
```

```
    % ROI=current_save(end).roi.mask;
    ROI(current_save(end).roi.mask)=1;
end

ROI(ROI==0)=NaN;
figure1=figure(1);
axes1 = axes('Parent',figure1);
hold(axes1,'on');
surf(ROI,'Parent',axes1,'LineStyle','none','FaceAlpha',0.5);
title('ROI')
xlabel('x axis')
ylabel('y axis')
zlabel('ROI logical')

imshow(img)

view(2)
colormap(spring)
set(gca,'YDir','reverse')
axis(axes1,'ij')

Exx_mean=zeros(k,1);
% Exx_std=zeros(k,1);
% Exx_median=zeros(k,1);
Eyy_mean=zeros(k,1);
Eyy_std=zeros(k,1);
Eyy_median=zeros(k,1);
Exy_mean=zeros(k,1);
Poisson_mean=zeros(k,1);

Lxx_mean=zeros(k,1);
Lxx_std=zeros(k,1);
```

```
Lyy_mean=zeros(k,1);
Lyy_std=zeros(k,1);

Eyy_log_mean=zeros(k,1);
Eyy_log_std=zeros(k,1);
Eyy_log_min=zeros(k,1);
Eyy_log_max=zeros(k,1);
% Per ogni immagine, calcolo la dimensione del ROI (che varia e diventa
% sempre più piccolo man mano che esce dal'immagine)
% Se provo con un ROI più piccolo, le dimensioni del ROI rimangono fisse
for i=1:k
if strcmp(Config,'Lagrange')
% Green-Lagrange strain (reference ROI)
Exx=data_dic_save.strains(i).plot_exx_ref_formatted;
Eyy=data_dic_save.strains(i).plot_eyy_ref_formatted;
Exy=data_dic_save.strains(i).plot_exy_ref_formatted;

Eyy_log(i,:,:)=log(sqrt(2*Eyy+1));
Eyy_log(Eyy_log==0)=NaN;

% U=data_dic_save.displacements(i).plot_u_ref_formatted;
% V=data_dic_save.displacements(i).plot_v_ref_formatted;

Poisson=-log(sqrt(2*Exx+1))./log(sqrt(2*Eyy+1));
% Poisson(isnan(Poisson))=0;

maschera=data_dic_save.strains(i).roi_ref_formatted.mask;
end
if strcmp(Config,'Eulero')
% Almansi-Eulero strain (current ROI)
Exx=data_dic_save.strains(i).plot_exx_cur_formatted;
Eyy=data_dic_save.strains(i).plot_eyy_cur_formatted;
```

```
Exy=data_dic_save.strains(i).plot_exy_cur_formatted;

Eyy_log(i,:,:)=log(sqrt(1./(1-2*Eyy)));
Eyy_log(Eyy_log==0)=NaN;

% U=data_dic_save.displacements(i).plot_u_cur_formatted;
% V=data_dic_save.displacements(i).plot_v_cur_formatted;

Poisson=-log(sqrt(1./(1-2*Exx)))./log(sqrt(1./(1-2*Eyy)));
% Poisson(isnan(Poisson))=0;

maschera=data_dic_save.strains(i).roi_cur_formatted.mask;
end

Exx_iter=Exx(maschera);
Eyy_iter=Eyy(maschera);
Exy_iter=Exy(maschera);

Exx_mean(i,1)=mean(Exx_iter);
% Exx_std(i,1)=std(Exx_iter);
% Exx_median(i,1)=median(Exx_iter);
Eyy_mean(i,1)=mean(Eyy_iter);
Eyy_std(i,1)=std(Eyy_iter);
Eyy_median(i,1)=median(Eyy_iter);
Exy_mean(i,1)=mean(Exy_iter);

%%%
if strcmp(Config,'Lagrange')
% Green-Lagrange strain (reference ROI)
Lxx_iter=2*Exx_iter+1;
Lyy_iter=2*Eyy_iter+1;
end
```

```
if strcmp(Config,'Eulero')
% Almansi-Eulero strain (current ROI)
Lxx_iter=1./(1-2*Exx_iter);
Lyy_iter=1./(1-2*Eyy_iter);
end

Poisson_iter=-log(sqrt(Lxx_iter))./log(sqrt(Lyy_iter));
% I=find((Poisson_iter>=-1)&(Poisson_iter<=0.5));
I=find((Poisson_iter>=0)&(Poisson_iter<=0.5));
Poisson_mean(i,1)=mean(Poisson_iter(I));

if i==k
    figure2=figure(2);
    Poisson(Poisson==0)=NaN;
%     Poisson((Poisson<-1)|(Poisson>0.5))=NaN;
    Poisson((Poisson<0)|(Poisson>0.5))=NaN;

    axes1 = axes('Parent',figure2);
    hold(axes1,'on');
    surf(Poisson,'Parent',axes1,'LineStyle','none')
    title('Poisson value')
    xlabel('x axis')
    ylabel('y axis')
    zlabel('Poisson')
    view(2)
    colormap(jet)
    set(gca, 'YDir','reverse')
    axis(axes1,'ij');
    colorbar('peer',axes1);
    % set(axes1,'XColor',[0.941176474094391 0.941176474094391 0.941176474094391],...
    %     'YColor',[0.941176474094391 0.941176474094391 0.941176474094391],'ZColor',...
    %     [0.941176474094391 0.941176474094391 0.941176474094391]);
end
```

```
Lxx_mean(i,1)=mean(Lxx_iter);
Lxx_std(i,1)=std(Lxx_iter);
Lyy_mean(i,1)=mean(Lyy_iter);
Lyy_std(i,1)=std(Lyy_iter);

Eyy_log_iter=log(sqrt(Lyy_iter));
Eyy_log_mean(i,1)=mean(Eyy_log_iter);
Eyy_log_std(i,1)=std(Eyy_log_iter);
Eyy_log_min(i,1)=min(Eyy_log_iter);
Eyy_log_max(i,1)=max(Eyy_log_iter);
end
% Exx_mean
% Exx_std
% Exx_median
% Eyy_mean
% Eyy_std
% Eyy_median
% Exy_mean

Lxx_mean
% Lxx_std
Lyy_mean
% Lyy_std

Eyy_log_mean
Eyy_log_std
Eyy_log_min
Eyy_log_max

Poisson_mean

Poisson2=-log(sqrt(Lxx_mean))./log(sqrt(Lyy_mean))
```

```
figure(3)
plot(Eyy_log_mean,'b','linewidth',2)
title('Eyy_l_o_g strain curve')
xlabel('# image')
ylabel('Eyy_l_o_g (mm/mm)')

figure4=figure(4);
Eyy(Eyy==0)=NaN;
Eyy_log_show(:,:)=Eyy_log(time,:,:);
axes2 = axes('Parent',figure4);
hold(axes2,'on');
% surf(Eyy_log_show,'Parent',axes2,'LineStyle','none')
Zscaled = resizem(Eyy_log_show,spac+1);
surf(Zscaled,'Parent',axes2,'LineStyle','none')
% surf(Eyy,'Parent',axes2,'LineStyle','none')
if strcmp(Config,'Lagrange')
    title('\epsilon_Y_Y^l^a^g','FontSize',14,'FontWeight','bold')
end
if strcmp(Config,'Eulero')
    title('\epsilon_Y_Y^e^u^l','FontSize',14,'FontWeight','bold')
end
xlabel('X axis','FontSize',14,'FontWeight','bold')
ylabel('Y axis','FontSize',14,'FontWeight','bold')
zlabel('\epsilon_Y_Y','FontSize',14,'FontWeight','bold')
view(2)
colormap(jet)
set(gca, 'YDir','reverse')
axis(axes2,'ij');
colorbar('peer',axes2,'FontSize',14,'FontWeight','bold');
a=min(min(Eyy_log_show));
b=max(max(Eyy_log_show));
```

```
% a=min(min(Eyy));
% b=max(max(Eyy));
caxis([a b])

% J = imresize(img,1/(spac+1));
% im=imshow(J);
im=imshow(img);
im.AlphaData = 0.4;

figure5=figure(5);
DEyy_Dy_mean=zeros(k,1);
DEyy_Dy_std=zeros(k,1);
DEyy_Dy_min=zeros(k,1);
DEyy_Dy_max=zeros(k,1);
for i=1:k
Eyy_log_grad(:,:)=Eyy_log(i,:,:);
[DEyy_Dx(i,:,:),DEyy_Dy(i,:,:)] = gradient(Eyy_log_grad,spac,spac);
% DEyy_Dy(abs(DEyy_Dy)>=0.1)=NaN;

I=isnan(DEyy_Dy(i,:,:));

DEyy_Dy_iter=DEyy_Dy(i,I==0);
DEyy_Dy_mean(i)=mean(DEyy_Dy_iter);
DEyy_Dy_std(i)=std(DEyy_Dy_iter);
DEyy_Dy_min(i)=min(DEyy_Dy_iter);
DEyy_Dy_max(i)=max(DEyy_Dy_iter);
end
DEyy_Dy_mean
DEyy_Dy_std
DEyy_Dy_min
DEyy_Dy_max
```

```
DEyy_Dy_mean_mean=mean(DEyy_Dy_mean)
DEyy_Dy_mean_std=std(DEyy_Dy_mean)

axes3 = axes('Parent',figure5);
hold(axes3,'on');

DEyy_Dy_show(:,:)=DEyy_Dy(time,:,:);
Zscaled = resizem(DEyy_Dy_show,spac+1);

% surf(DEyy_Dy_show,'Parent',axes3,'LineStyle','none','FaceAlpha',1);
surf(Zscaled,'Parent',axes3,'LineStyle','none','FaceAlpha',1);
if strcmp(Config,'Lagrange')
    title('Gradient field of \partial\epsilon_Y_Y^l^a^g/\partialY','FontSize',14,'FontW
end
if strcmp(Config,'Eulero')
    title('Gradient field of \partial\epsilon_Y_Y^e^u^l/\partialY','FontSize',14,'FontW
end

xlabel('X axis','FontSize',14,'FontWeight','bold')
ylabel('Y axis','FontSize',14,'FontWeight','bold')
zlabel('\Delta\epsilon_Y_Y/dy','FontSize',14,'FontWeight','bold')
view(2)
colormap(jet)
set(gca,'YDir','reverse')
axis(axes3,'ij')
colorbar('peer',axes3,'FontSize',14,'FontWeight','bold')
a=min(min(DEyy_Dy_show));
b=max(max(DEyy_Dy_show));
caxis([a b])
% J = imresize(img,1/(spac+1));
% im=imshow(J);
im=imshow(img);
im.AlphaData = 0.4;
```

Bibliography

[1] Bottega W.J., Bishay P.L., “On the mechanics of a detaching retina”, Mathematical medicine and biology, 2012

[2] Chen K., Weiland J.D., “Anisotropic and inhomogeneous mechanical characteristics of the retina”, Journal of Biomechanics, Elsevier Ltd., 2010, 1417-1421

[3] Chen K., Weiland J.D., “Mechanical characteristics of the porcine retina in low temperatures”, In: “Retina, the journal of retinal and vitreous diseases”, Volume 32, Number 4, 2012, pp 844 – 847

[4] Cioffi G.A., Granstam E., Alm A., “Ocular circulation”, In: “Adler’s Physiology of the Eye”, Kaufman P.L., Alm A. (eds.), 10th edn, pp. 747–784, Mosby, St Louis 2003.

[5] Cook C., Sulik K.K., Wright K.W., “Embryology”, In: “Pediatric Ophthalmology and Strabismus”, Wright K.W., Spiegel P.H. (eds), 2nd edition, pp 3-38, 2003

[6] Cunha-Vaz J.G., “The blood-retinal barriers system”, Basic concepts and clinical evaluation. Review. Exp. Eye Res. 78, 715–721, 2004

[7] Cunha-Vaz J.G., “The blood-ocular barriers”, Surv. Ophthalmol, 23, 279–296, 1979

[8] Davis J.R., “Tensile Testing”, 2nd edition, ASM International, 2004

[9] Duke-Elder S., Cook C., “Normal and abnormal development. Part 1. Embryology, In: System of Ophthalmology”, Vol. 3, Duke-Elder S. (eds.), Henry Kimpton, pp 190-201, 1963

[10] "Facts About Retinal Detachment", National Eye Institute, October 2009

[11] Fraser S., "Retinal detachment", BMJ Clinical Evidence, 2010

[12] Hatef E., Sena DF., Fallano KA., Crews J., Do DV., "Pneumatic retinopexy versus scleral buckle for repairing simple rhegmatogenous retinal detachments", 2015

[13] Haug SJ., Bhisitkul RB., "Risk factors for retinal detachment following cataract surgery", 2012

[14] Hildebrand G.D., Fielder A.R., “Anatomy and Physiology of the Retina”, In. “Pediatric Retina”, Reynolds J., Olitsky S. (eds), Springer-Verlag Berlin Heildelberg, pp 39-60, 2011

[15] Kanski J.J., Milewski S.A., “Introduction”, In: “Diseases of the Macula”, Kanski J.J., Milewski S.A. (eds.), pp. 1–18. Mosby, St Louis, 2002

[16] Levin L.A., “Optic nerve”, In: “Adler’s Physiology of the Eye”, Kaufman P.L., Alm A. (eds.), 10th edn, pp. 603–638. Mosby, St Louis, 2003

[17] Lionello G. *et al.,* “An effective procedure to create a speckle pattern on biological soft tissue for digital image correlation measurements”, Journal of the mechanical behavior of biomedical materials, Elsevier, Number 39, 2014, 1-8

[18] Mann I., “The development of the human eye”, 3rd edition, British Medical Association, 1964

[19] Olsen T. *et al*., “Porcine sclera: thickness and surface area”, Investigative Ophthalmology and visual science, Arvo Journals, Volume 43, Issue 8, 2002

[20] Roof D.J., Makino C.L., “The structure and function of retinal photoreceptors”, In: “Principles and Practice of Ophthalmology”, Albert D.A., Jakobiec F.A. (eds.), 2nd edn, pp. 1624–1673, Saunders, Philadelphia, 2000

[21] "Sensory Reception: Human Vision: Structure and function of the Human Eye", vol. 27, Encyclopædia Britannica, 1987

[22] Strauss O., “The retinal pigment epithelium in visual function”, Physiol. Rev. 85, 845–881, 2005

[23] Tessier-Lavigne M., “Visual processing by the retina”, In: “Principles of Neural Science”, Kandel E.R., Schwartz J.H., Jessell T.M. (eds.), 4th edn, pp. 507–522, McGraw-Hill, New York, 2000

[24] Thumann G., Hoffmann S., Hinton D.R., “Cell biology of the retinal pigment epithelium”, In: “Retina”, Ryan S.J. (ed), 4th (ed), pp. 137–152, Elsevier-Mosby, St. Louis, 2006

[25] Wollensak G., Spoerl E., “Biomechanical characteristics of retina”, In: “Retina, the journal of retina and vitreous diseses”, Volume 24, Number 6, 2004, pp 967-970

[26] Wu W., et al., “Basic Mechanical Properties of retina in simple elongation”, J Biomedical Eng, 1987,109: 65-67

[27] Wurtz R.H., Kandel E.R., “Central visual pathways”, In: “Principles of Neural Science”, Kandel E.R., Schwartz J.H., Jessell T.M. (eds.), 4th edn, pp. 523–547, McGraw-Hill, New York, 2000

[28] Yanoff M., Duker J.S., “Ophthalmology”, 3rd edition. Edinburgh: Mosby, p 725

[29] Yu DY., Yu PK., Cringle SJ., Kang MH., Su EN., "Functional and morphological characteristics of the retinal and choroidal vasculature". Progress in Retinal and Eye Research, 2014

[30] Znaor L., Medic A., Binder S., Vucinovic A., Marin Lovric J., Puljak L., "Pars plana vitrectomy versus scleral buckling for repairing simple rhegmatogenous retinal detachments", 2019